

## INFORMATION TO USERS

This manuscript has been reproduced from the microfilm master. UMI films the text directly from the original or copy submitted. Thus, some thesis and dissertation copies are in typewriter face, while others may be from any type of computer printer.

**The quality of this reproduction is dependent upon the quality of the copy submitted.** Broken or indistinct print, colored or poor quality illustrations and photographs, print bleedthrough, substandard margins, and improper alignment can adversely affect reproduction.

In the unlikely event that the author did not send UMI a complete manuscript and there are missing pages, these will be noted. Also, if unauthorized copyright material had to be removed, a note will indicate the deletion.

Oversize materials (e.g., maps, drawings, charts) are reproduced by sectioning the original, beginning at the upper left-hand corner and continuing from left to right in equal sections with small overlaps. Each original is also photographed in one exposure and is included in reduced form at the back of the book.

Photographs included in the original manuscript have been reproduced xerographically in this copy. Higher quality 6" x 9" black and white photographic prints are available for any photographs or illustrations appearing in this copy for an additional charge. Contact UMI directly to order.

**UMI<sup>®</sup>**

Bell & Howell Information and Learning  
300 North Zeeb Road, Ann Arbor, MI 48106-1346 USA  
800-521-0600



A STUDY OF TWO OPEN CLUSTERS CONTAINING WOLF-RAYET STARS

by

Stephen L. Shorlin

A THESIS SUBMITTED IN PARTIAL  
FULFILLMENT OF THE REQUIREMENTS  
FOR THE DEGREE OF  
MASTER OF SCIENCE

DEPARTMENT OF ASTRONOMY AND PHYSICS  
SAINT MARY'S UNIVERSITY  
MAY 1998

HALIFAX, NOVA SCOTIA

©Stephen L. Shorlin, 1998



National Library  
of Canada

Acquisitions and  
Bibliographic Services

395 Wellington Street  
Ottawa ON K1A 0N4  
Canada

Bibliothèque nationale  
du Canada

Acquisitions et  
services bibliographiques

395, rue Wellington  
Ottawa ON K1A 0N4  
Canada

*Your file Votre référence*

*Our file Notre référence*

The author has granted a non-exclusive licence allowing the National Library of Canada to reproduce, loan, distribute or sell copies of this thesis in microform, paper or electronic formats.

The author retains ownership of the copyright in this thesis. Neither the thesis nor substantial extracts from it may be printed or otherwise reproduced without the author's permission.

L'auteur a accordé une licence non exclusive permettant à la Bibliothèque nationale du Canada de reproduire, prêter, distribuer ou vendre des copies de cette thèse sous la forme de microfiche/film, de reproduction sur papier ou sur format électronique.

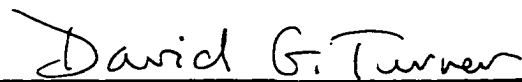
L'auteur conserve la propriété du droit d'auteur qui protège cette thèse. Ni la thèse ni des extraits substantiels de celle-ci ne doivent être imprimés ou autrement reproduits sans son autorisation.

0-612-40358-0

**Canada**

## Certificate of Examination

Saint Mary's University  
Department of Astronomy and Physics



---

Dr. David G. Turner  
Professor  
Department of Astronomy and Physics  
Saint Mary's University  
(Supervisor)



---

Dr. George F. Mitchell  
Professor  
Department of Astronomy and Physics  
Saint Mary's University



---

Dr. Michael J. West  
Professor  
Department of Astronomy and Physics  
Saint Mary's University



---

Dr. Robert J. Havlen  
Executive Director  
Astronomical Society of the Pacific  
San Francisco, CA

## Abstract

The results of *UBV* CCD photometry are presented for a newly discovered open cluster, as well as new photometry for thirty-seven members of the open cluster HM 1. The new open cluster, to be designated OCL 1104-610, has a distance modulus of  $V_o - M_V = 15.5 \pm 0.2$ , corresponding to a distance of  $12.6 \pm_{1.1}^{1.2}$  kpc, and is several Myr old. Members of the distant cluster include two Wolf-Rayet (WR) stars, WR 38 and WR 38a. WR 38 is the first WC4 star identified in an open cluster, and has been found to have an absolute magnitude  $M_v = -5.1$ , two magnitudes brighter than has been suspected for WC4 stars. WR 38a has an absolute magnitude  $M_v = -4.4$ , in agreement with other WN6 stars. Intrinsic colours of both WR stars are uncertain given the faintness of cluster members. HM 1 has been determined to have a distance modulus of  $V_o - M_V = 13.19 \pm 0.16$ , corresponding to a distance of  $4.34 \pm_{0.31}^{0.33}$  kpc. Its WR members, WR 87 and WR 89, have been found to be intrinsically slightly brighter and bluer than on average for WN7 stars, but not unreasonably so. In addition, photometry is presented for a third group of stars which possibly comprise an open cluster. The third cluster, to be designated OCL 1103-610, lies at a distance of  $V_o - M_V = 12.02 \pm 0.06$  and is 77 Myr old.

## Acknowledgements

I wish to thank my supervisor Dr. David Turner for his invaluable instruction, advice and patience, as well as for providing the opportunity to travel to Chile. I also wish to thank Boyd Duffee and the other astronomers and staff at UTSO and Las Campanas Observatories who made it possible for me to make the observations.

I must also thank everyone at Saint Mary's who made my experiences there educational, enjoyable and memorable. From professors to officemates, you helped make my first work as a graduate student and an astronomer as good an experience as it turned out to be. I'm very happy to be associated with you and the department.

Finally I thank Kelly Shorlin for her love and support. Thank you for washing dishes while I (ostensibly) finished. Thank you for all the boots in the right direction.

# Contents

Certificate of Examination	ii
Abstract	iii
Acknowledgements	iv
List of Figures	vi
List of Tables	viii
<b>1 Introduction</b>	<b>1</b>
<b>2 Observations and Image Processing</b>	<b>5</b>
2.1 Observations . . . . .	5
2.2 Image processing . . . . .	10
<b>3 Data Reduction</b>	<b>12</b>
3.1 Photometry . . . . .	12
3.2 Calibrating Photometry . . . . .	14
3.2.1 Potential systematic errors in $U-B$ . . . . .	17
<b>4 HM 1</b>	<b>28</b>
4.1 Extinction . . . . .	28
4.2 Star Counts . . . . .	30
4.3 Colour-colour diagram . . . . .	31
4.4 Reddening . . . . .	32
4.5 Variable-Extinction Diagram . . . . .	34
4.6 Colour-magnitude diagram . . . . .	38

<b>5 Distant Cluster</b>	<b>42</b>
5.1 Extinction . . . . .	42
5.2 Star Counts . . . . .	42
5.3 Colour-colour diagram . . . . .	43
5.4 Variable-Extinction Diagram . . . . .	45
5.5 Colour-magnitude diagram . . . . .	45
<b>6 The Wolf-Rayet Stars</b>	<b>49</b>
6.1 Photometry and Intrinsic Parameters . . . . .	49
6.1.1 WR 38 . . . . .	51
6.1.2 WR 38a . . . . .	52
6.1.3 WR 87 and WR 89 . . . . .	54
6.2 Conclusions . . . . .	55
<b>A HM 1 data</b>	<b>58</b>
<b>B Photometric data for Carina region stars</b>	<b>63</b>
<b>C Possible Carina cluster</b>	<b>69</b>
C.1 Extinction . . . . .	69
C.2 Star Counts . . . . .	69
C.3 Colour-colour diagram . . . . .	75
C.4 Variable-Extinction Diagram . . . . .	78
C.5 Colour-magnitude diagram . . . . .	82
<b>References</b>	<b>87</b>
<b>Vita</b>	<b>91</b>

## List of Figures

2.1	The HM 1 region . . . . .	8
2.2	The Carina region . . . . .	9
3.1	Discrepancy in UTSO $U-B$ data as a function of spectral type	20
3.2	HM 1 region finder chart . . . . .	23
3.3	Carina region finder chart . . . . .	24
3.4	Carina region finder chart inset . . . . .	25
3.5	Standard deviation in magnitude between exposures in $V$ , $B$ , and $U$ for the HM 1 field . . . . .	26
3.6	Standard deviation in magnitude between exposures in $V$ , $B$ , and $U$ for the Carina field . . . . .	27
4.1	Colour-colour diagram for HM 1 region . . . . .	33
4.2	Reddening Map of HM 1 . . . . .	35
4.3	Variable extinction diagram for HM 1 . . . . .	37
4.4	Colour Magnitude Diagram for HM 1 stars . . . . .	41
5.1	Uncorrected colour-colour diagram for the Carina region . . .	44
5.2	Variable extinction diagram for the Carina region . . . . .	46
5.3	Colour Magnitude Diagram for Distant Cluster . . . . .	47
C.1	$E_{U-B}$ vs. $E_{B-V}$ in the Carina region . . . . .	70
C.2	Strip counts in east/west direction for the Carina region . . . .	72
C.3	Strip counts in north/south direction for the Carina region . .	73
C.4	Ring counts for the Carina region . . . . .	74
C.5	Uncorrected colour-colour diagram for the Carina region . . .	76
C.6	Corrected colour-colour diagram for the Carina region . . . . .	77
C.7	Variable extinction diagram for the Carina region . . . . .	79

C.8	Reddening Map of the Carina region . . . . .	81
C.9	Colour Magnitude Diagram for the Carina region . . . . .	83
C.10	CMD for the Carina region with stars categorized by colour excess . . . . .	84
C.11	CMD for Carina region cluster members with overlaid isochrone	86

## List of Tables

1	Observation log . . . . .	7
2	Standard photometric data for the Carina region. . . . .	15
3	Spectral types and inferred intrinsic colours, absolute magnitudes and colour excesses for stars in HM 1 . . . . .	30
4	Photometry for members of HM 1 used to estimate $V_o - M_V$ . . . . .	39
5	Intrinsic parameters from the literature for relevant WR subtypes . . . . .	50
6	Photometric and derived intrinsic properties of WR 38 . . . . .	52
7	Photometric and derived intrinsic properties of WR 38a . . . . .	53
8	Photometric and derived intrinsic properties of WR 87 . . . . .	54
9	Photometric and derived intrinsic properties of WR 89 . . . . .	55
10	Photometric data for stars in the region of HM 1 . . . . .	62
11	Photometric data for stars in the distant cluster in the Carina field . . . . .	63
12	Photometric data for stars in the Carina region . . . . .	68
13	Photometric data for stars in the Carina region used to estimate $V_o - M_V$ . . . . .	80

# Chapter 1

## Introduction

Wolf-Rayet (WR) stars are characterized by spectra with strong broad emission lines that provide evidence of products of either hydrogen or helium burning at their surfaces. It is generally accepted that WR stars are a late stage of the evolution of the most massive stars. Large mass loss rates of several  $10^{-5} M_{\odot}/\text{yr}$  are thought to be responsible for stripping massive, hot stars of their outer layer of hydrogen, revealing core materials that produce the WR phenomenon as a result of strong stellar winds.

WR stars have been classified according to their spectra based on the strengths of nitrogen, carbon and oxygen lines, thus defining the WN, WC and WO spectral types. Subtypes have also been created based on relative strengths of lines of each species as well as the appearance of lines of other species. Subtypes are classified numerically as in the MK classification scheme, with the lowest numbered subtypes referred to as “early” and the highest numbered referred to as “late”. As in the MK scheme, spectra of early-type stars indicate higher temperatures than those of late-type stars.

The late WN-type stars (WNL: WN7-WN11) have Balmer lines in their spectra whereas the early WN-type stars (WNE: WN4-WN6) do not, thus roughly indicating an evolutionary sequence: WNL evolves to WNE as hydrogen is lost in the stellar wind. The WC and WO stars show the products of helium burning and are accepted to be more evolved than the WN stars. WC stars evolve from late (WCL) to early (WCE) subtypes as well, with the WO stage being the extreme extension of the earliest WC stars. The general evolutionary scheme is  $O \rightarrow \text{WNL} \rightarrow \text{WNE} \rightarrow \text{WCL} \rightarrow \text{WCE}$ , although the exact

entry point into the WR sequence, as well as the time spent in each subtype, is dependent upon the mass of the O-star progenitor and the mass-loss rate in each phase.

The WR classification system was initially created in an attempt to classify the stars solely on the basis of effective temperature and luminosity, as in the MK system. Unfortunately, the emission lines used to classify the stars are created in the optically thick stellar winds, and thus a WR star's spectral type reflects the temperature and ionization in its winds. A more detailed scheme to reflect actual stellar properties has been introduced by Smith *et al.* (1996). Since the majority of past studies, however, have been done prior to the introduction of the new system, all quoted WR spectral types and comparisons with stars of similar spectral type in this thesis are based upon the original classification system.

As a recognizable and classifiable stage in the evolution of the most massive and short-lived of stars, WR stars allow one to study many astrophysically interesting problems. The high sensitivity of the evolution of massive stars to parameters such as mass loss may be constrained by determining how observed WR stars fit within different evolutionary scenarios. WR stars can also be used as spiral arm tracers as they are the products of very recent star formation. As well, they are interesting as the possible progenitors of type Ib and Ic supernovae, although this is still a matter of debate (Conti 1996).

In order to use WR stars as astronomical and astrophysical tracers and tests of stellar evolution theory, information on their intrinsic parameters of absolute magnitude and intrinsic colour is necessary. One way of deter-

mining intrinsic WR parameters without *a priori* assumptions is to study WR stars in open clusters and associations. Recent estimates are that 24 of the 201 known Galactic WR stars are members of open clusters while 24 more are members of identified associations. Membership of a WR star in a group of stars with a measurable distance and reddening allows one to transform the observed parameters of apparent magnitude and colour to absolute magnitude and intrinsic colour.

This thesis deals primarily with the photometry of two open clusters which each have two WR members. One has been previously studied photometrically and new photometry, as well as photometric data for fainter member stars, are used here to provide a new analysis of the cluster distance and reddening. The second open cluster is a new discovery and photometric data for its eight brightest members, including the two WR stars, provide an opportunity to determine its distance, as well as an estimate of its reddening. Analysis of data concerning a third region possibly containing an open cluster is included in Appendix A as a matter of completeness, but it is secondary to our main purpose of deriving intrinsic parameters for WR stars.

As steps in the photometric process, the details of CCD image processing and data reduction are described in Sections 2.2 and 3.1. The transformation of instrumental magnitudes to a supposedly “standard” *UBV* system is also outlined as performed using existing cluster photometric data. The term “standard” *UBV* is used because problems in calibration resulting from the Balmer discontinuity in stellar spectral energy distributions often cause instrumental data to be reduced to some non-standard photometric system

which only approximately matches the true *UBV* system. Balmer discontinuity effects specific to the filter and detector system used in producing the data for this thesis are addressed in as complete a manner as possible, and the data presented have been corrected for such effects.

The analysis of the cluster data to derive parameters of extinction, size, distance, and age for each cluster is presented. Based upon the assumed membership of each WR star in its associated open cluster, the intrinsic parameters for our program objects have been derived and are included with comparisons to previous studies of the relevant spectral subclasses.

# Chapter 2

## Observations and Image Processing

### 2.1 Observations

The fields of observation were chosen in order to make new observations of a previously studied open cluster, as well as to ascertain the existence of a new open cluster, both associated with Wolf-Rayet stars. The previously studied open cluster, HM 1 (Havlen and Moffat 1977), contains two Wolf-Rayet members: WR 87 and WR 89. A previously unstudied region in Carina is centred on  $l = 290^{\circ}58$ ,  $b = -0^{\circ}94$ . It was suggested for study to the author by Dr. D. Turner. It seemed a likely candidate for an open cluster as there was an apparent surplus of stars in the region according to Digitized Sky Survey frames. Preliminary photoelectric photometry of the brightest stars indicated a sequence of stars in colour and magnitude that might constitute an open cluster. Also, there were three Wolf-Rayet stars in the vicinity: WR 37, WR 38 and WR 39 at  $6.8'$ ,  $1.4'$  and  $3.8'$ , respectively, from apparent cluster centre. Observations were planned to image the apparent cluster as well as all three WR stars. Weather conditions at the observing site made it impossible to image WR 37 and WR 39, however. Although it was not known at the time of observation, there is a fourth Wolf-Rayet star, WR 38a, within less than half an arcminute of WR 38 and thus it was imaged with the cluster region. WR 38a was discovered in a more recent deep search for WR stars (Shara *et al.* 1991) and was not included in the catalogues used to design the observation program.

Data were obtained at the University of Toronto Southern Observatory

(UTSO) between June 7 and 18, 1996. The observations were made with the 60-cm Helen Sawyer Hogg Telescope using the METACHROME coated  $512 \times 512$  PM512 CCD, which has a  $4' \times 4'$  field. The CCD chip was cooled by liquid nitrogen for all observations. A “standard” set of *UBV* filters was employed.

Long and short exposures in each of *U*, *B*, and *V* were taken for each pointing of the telescope. The definition of the terms “long” and “short” are somewhat ambiguous, as they were determined by the transparency and seeing conditions at the time of each exposure. The HM 1 region was divided into a central region, surrounded by northeast, southeast, and southwest regions as seen in Figure 2.1. The Carina region was divided into east and west regions as seen in Figure 2.2. Figures 2.1 and 2.2 have been created from STScI Digitized Sky Survey images. Images were taken of the northwest region as well, but data from those images were not reduced because of a lack of standards in the northwest field. The observation log is reproduced in Table 1.

Variable transparency conditions during each evening’s run made it difficult to use external standards to calibrate the photometry. Therefore, it was decided to use stars in each field that had existing photoelectric data as the basis for the data reduction. This is why no additional stars, other than those in the studied fields, were observed.

Variable transparency also made it difficult to make long exposures. The relatively poor blue sensitivity of the CCD called for long exposures when making exposures in *U*, yet the exposure times were limited by guiding. Guiding was done with an ST4 autoguider that was centred on a star in the

Carina Region June 17							
Filter	Exp time (s)	Pos.		Filter	Exp t (s)	Pos.	
<i>U</i>	600	E					
<i>U</i>	1200	E					
<i>B</i>	120	E					
<i>B</i>	500	E					
<i>V</i>	20	E					
<i>V</i>	120	E					
<i>U</i>	600	W					
<i>U</i>	1200	W					
<i>B</i>	90	W					
<i>B</i>	300	W					
<i>V</i>	30	W					
<i>V</i>	120	W					

HM 1							
Date	Filter	Exp t (s)	Pos.	Date	Filter	Exp t (s)	Pos.
June 7	<i>V</i>	10	Cent	June 11	<i>B</i>	180	SW
June 7	<i>V</i>	60	Cent	June 11	<i>B</i>	500	SW
June 7	<i>B</i>	30	Cent	June 16	<i>U</i>	600	SE
June 7	<i>B</i>	250	Cent	June 16	<i>U</i>	1200	SE
June 7	<i>U</i>	200	Cent	June 16	<i>V</i>	10	NE
June 7	<i>U</i>	1200	Cent	June 16	<i>V</i>	60	NE
June 9	<i>V</i>	20	SE	June 16	<i>B</i>	120	NE
June 9	<i>V</i>	120	SE	June 16	<i>B</i>	600	NE
June 9	<i>B</i>	300	SE	June 18	<i>U</i>	600	SW
June 9	<i>B</i>	900	SE	June 18	<i>U</i>	1200	SW
June 11	<i>V</i>	20	SW	June 18	<i>U</i>	1200	NE
June 11	<i>V</i>	60	SW	June 18	<i>U</i>	600	NE

Table 1: Observation log

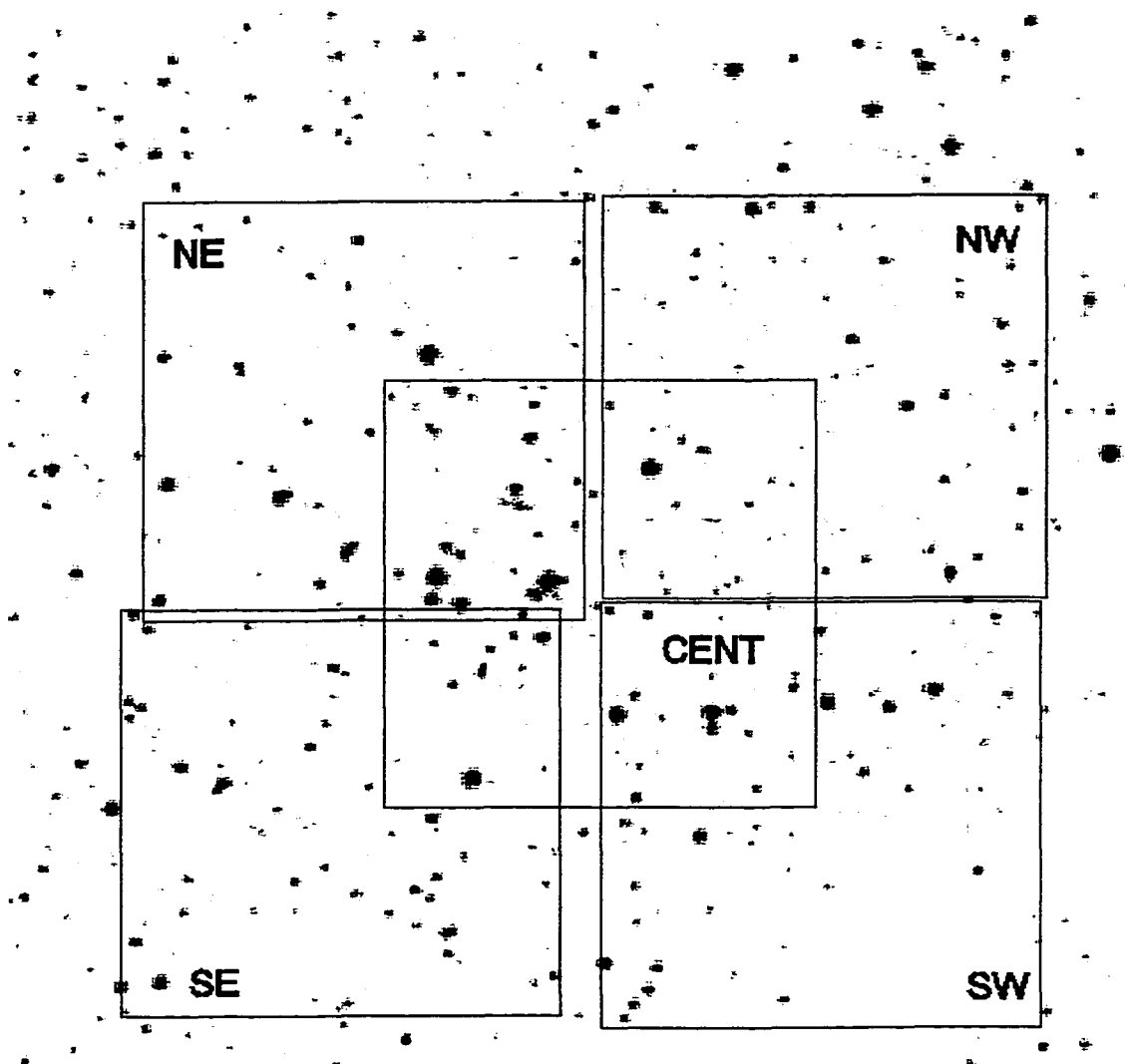


Figure 2.1: The HM 1 region. The squares are  $4' \times 4'$ . North is up and east is to the left.

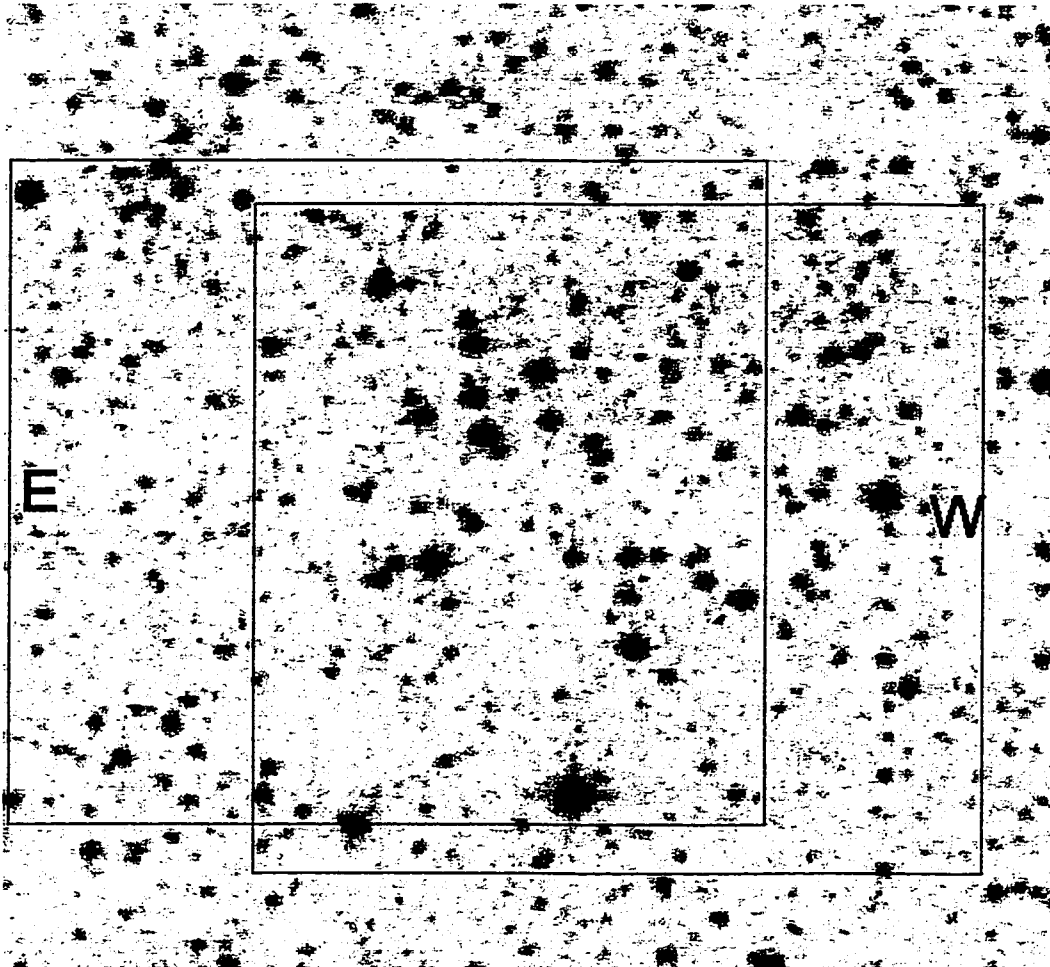


Figure 2.2: The Carina region. The squares are  $4' \times 4'$ . North is up and east is to the left.

field at the beginning of an exposure. At times, the guider would “lose” a star when the cloud conditions became thick enough. When that happened, the guider would automatically begin moving the secondary in a step-search pattern to “find” the image. If the duration of cloud cover was significantly long, the exposure would be ruined. After some experimentation and through consultation with the resident astronomer, it was decided that 1200s exposures were the longest that could be made while reasonably expecting to complete the exposure.

Sets of ten bias (zero-second) exposures were taken at the beginning and end of each night. As a precaution against light-leak, they were taken with the shutter closed and the  $U$  filter in place. As well, flat-field images for each of  $U$ ,  $B$ , and  $V$  were taken for each night. These were captured by imaging a section of the dome painted blue, illuminated by a bright lamp, while focused for stellar imaging. The exposure time for each was selected so that peak intensity was approximately three-quarters the saturation level of the CCD. Since the CCD was liquid nitrogen cooled, it was unnecessary to take any dark current frames for processing.

## 2.2 Image processing

The image capture software at UTSO stored the images as FITS files, and assigned each a FITS header with most of the necessary data contained in keywords. One keyword not assigned, yet necessary for image processing under IRAF, was *data-typ*. This keyword denoted the type of image file: object, bias or flat-field. It was added to the FITS headers, and assigned correctly in each case, by using the `hedit` command. The identifiers were *object* for object frames, *zero* for bias frames and *flat* for flat-fields. All image

processing was done using IRAF with the **ccdred** package of commands.

The bias images at the beginning and end of each night's run were examined using the **imexamine** task. It was determined that there were no detectable changes in either bias level or pattern during each night. The bias images were then median-combined using the **zerocombine** command.

The flat-field images were corrected for their bias level using the **ccdproc** command. **ccdproc** was run with only the bias level correction set to be used, and the combined bias image for the appropriate night indicated. The flat-fields in each of  $U$ ,  $B$ , and  $V$  were then average-combined using the task **flatcombine**. The object images for each night were then analyzed with **ccdproc**, with both bias and flat-field correction set to be used and with the appropriate bias and flat-field images indicated.

Artifacts attributable to cosmic ray hits on the CCD were evident on most frames, especially for longer exposures. An initial cleaning was performed using the **cosmicrays** command, which selects pixels for "cleaning" (replacement by the median value of surrounding pixels). When used, **cosmicrays** still left many artifacts untouched. They were much larger than single pixels and so were not detectable by the **cosmicrays** algorithm. They were subsequently removed using **imedit**. The two images of the same colour were **blinked**, and where an anomalous artifact was obvious, it was edited. With the task **imedit** the cursor was placed over the image display at the position of an artifact, and a circular aperture was selected. Pixel values inside the aperture were then replaced by values determined by a larger annulus. This editing was done for each frame.

# Chapter 3

## Data Reduction

### 3.1 Photometry

Determinations of instrumental *UBV* magnitudes for stars imaged in each region were done using `daophot` under IRAF essentially as outlined by Massey and Davis (1992). Each frame was examined using `imexamine` in order to determine the full width at half-maximum (FWHM) for stellar images. As well, suitable background regions were chosen to examine the statistics of background light levels. The data were used as parameters for the `daofind` task, which automatically detected stars and wrote stellar coordinates to a file.

The `phot` task was then run on each frame to assign simple aperture photometry magnitudes to each star. They were calculated by using a small circular aperture, centred on each star's coordinates, in conjunction with a larger annulus to measure background levels. Values for the aperture and annulus size were chosen as suggested by Massey and Davis. The instrumental magnitudes were used as input for the more sophisticated `psf` photometry package.

Had the images been less crowded, simple aperture photometry would have been accurate. In the present case, stellar images often overlapped and more sophisticated means were necessary. The photometry was done using the `psf` task, which used uncrowded, bright stars as representatives of the stellar profiles for each frame. The routine `phot` generated magnitudes as measures of their brightness. Representative stars, known as *psfstars* were

chosen interactively during the **psf** session, and selected to be used only if they appeared to be “normal” stellar images (*i.e.*, no unremovable cosmic rays or nearby neighbours). The routine **psf** then generated an “average” stellar profile from such representatives to be applied to all stars in the frame.

To check the goodness of fit, the average psf was applied to the psfstars using the **nstar** and **substar** tasks. The task **nstar** examined the regions surrounding the psfstars for near neighbours which may have interfered with the construction of the average psf. The routine **substar** would then fit the average psf to the selected stars (psfstars and near neighbours) while minimizing residuals, thus assigning them instrumental magnitudes. The theoretical stellar profiles corresponding to the assigned magnitudes (and positions, when allowing for variability across the image) were then subtracted from the image frame. The new subtracted frame was then examined to evaluate the usefulness of the psfstars. Often, one or more stars had close neighbours or cosmic ray hits that could not be detected until the subtraction was performed. Such stars were deselected as psfstars during a second run of **psf**. The processes were repeated until the stellar images were subtracted cleanly, thus indicating a good average psf.

Once an appropriate psf was generated, the **allstar** task was run. This was essentially the same as **substar**, except that it was run for all stars on the frame, with the **phot** generated magnitude files as initial input. Again, a fit was made to the psf, minimizing residuals and accounting for variability if specified, to assign a unique instrumental magnitude to each star. The task **allstar** also performed a subtraction on all stars in the magnitude file. That allowed the author to determine whether some “stars” were actually

two or more star images very close together. If that was the case, the initial coordinate files were edited to include the new star coordinates and to delete the incorrect “star” positions.

When all stars in a frame were identified, the quality of the subtraction was evaluated. That qualitatively defined the goodness of fit of the psf, and also allowed for examination of individual stars. In several instances, cosmic rays images were missed during the editing process and showed up in the subtracted images. They could then be identified and removed from the images. When all stars were identified, the routines **phot** and **allstar** were rerun to obtain final instrumental magnitudes for each frame.

As a check, the routine **psf** was rerun for each frame with allowance for linear variability across the frame (the order of the psf was set to 1 in the **psf** parameter file). When the task **allstar** was run using the new, variable psf, the subtraction was often quite a bit worse than when the psf was constrained to be constant. The small number of available psfstars was the reason for that, as high weight was given to brighter stars near the edges. That skewed the shape of the psf to mimic their profiles, including noise, and not the general profile of stars on the frame.

## 3.2 Calibrating Photometry

The tasks in IRAF that are normally used for the transformation of instrumental magnitudes to a standard system were not useful here. Such tasks use standard *UBV* magnitudes and colours for some stars, as well as air masses for the exposures, to create transformation equations. As the seeing conditions were not photometric and the transparency variable during each night’s run, the air mass in the transformation equations would not have

Star	$V$	$B-V$	$U-B$
1	9.23	1.05	0.84
2	10.97	0.46	0.07
3	11.22	1.18	1.10
4	11.47	0.17	-0.04
5	11.69	0.08	-0.37
8	12.14	1.93	2.21
9	12.11	0.32	0.16
10	12.65	1.61	1.37
11	12.77	0.12	-0.32
16	13.55	0.56	0.27

Table 2: Standard photometric data for the Carina region.

been reliable. Therefore, a simple relation of the following form was used:

$$\Delta m = m_{\text{ins}} - m_{\text{std}} = a \cdot (B-V)_{\text{std}} + b, \quad (3.1)$$

where  $m_{\text{ins}}$  and  $m_{\text{std}}$  are the instrumental and standard magnitudes,  $(B-V)_{\text{std}}$  is the standard  $B-V$  colour and  $a$  and  $b$  are constants.

A fit to such a simple relation could not be made using existing IRAF tasks, so it was decided to perform a fit to the data using Microsoft Excel. The output from `allstar` was not immediately formatted for use in Excel, so a FORTRAN program was written to extract the useful data: an ID number, X and Y coordinates on the frame, instrumental magnitude and error estimate. The data files were then read in as text files to be used under Excel.

Photoelectric photometry by Pedreros (unpublished) was the basis for the standard  $UBV$  magnitudes of the Carina region stars. The photometric data are listed in Table 2. Photoelectric photometry by Havlen and Moffat (1977) was the basis for the standard  $UBV$  magnitudes for HM 1 stars. There were several problems with the quoted values in each set of standard data.

Several stars were revealed to have very nearby neighbours. The neighbour stars, while faint, may have contributed to anomalous differences between instrumental and standard magnitudes. That seems to have been the case for stars 2 and 9 in the Carina region and star 3 (HM #2) in HM 1. In the Carina region, star 1 was very bright and unusable as a standard owing to saturation and diffraction effects.

The relationship between  $\Delta m$  and  $(B-V)_{\text{std}}$  was plotted for each frame, and the parameters  $a$  and  $b$  determined using Excel tools. The data were then split into two data sets for each pointing: long and short. That provided  $U_{\text{ins}}$ ,  $B_{\text{ins}}$ , and  $V_{\text{ins}}$  values for the stars, and permitted a transformation to the standard system with relations of the form,

$$V_{\text{ins}} - V_{\text{std}} = a \cdot (B-V)_{\text{std}} + b \quad (3.2)$$

and

$$B_{\text{ins}} - B_{\text{std}} = c \cdot (B-V)_{\text{std}} + d. \quad (3.3)$$

Subtracting Equation 3.3 from 3.2 results in

$$(B-V)_{\text{ins}} - (B-V)_{\text{std}} = (c - a) \cdot (B-V)_{\text{std}} + d - b, \quad (3.4)$$

or rewriting

$$(B-V)_{\text{std}} = \frac{(B-V)_{\text{ins}} + b - d}{1 + c - a}. \quad (3.5)$$

The last result permitted the transformation of the instrumental  $B-V$  colours to a standard system, and such standard colours were used to transform the instrumental magnitudes for each filter as prescribed in Equation 3.1.

### 3.2.1 Potential systematic errors in $U-B$

The Balmer discontinuity is a feature in the continuum of stellar radiation that occurs at a wavelength of  $3646 \text{ \AA}$ . It is indicative of the longest wavelength of a photon that can be absorbed by neutral hydrogen in the first excited state. It arises because neutral hydrogen is a source of continuum opacity in stars. The degree to which hydrogen dominates as a source of opacity depends mostly upon temperature, especially when dealing with main sequence stars. The size of the Balmer discontinuity is therefore a function of spectral type and luminosity.

The Balmer discontinuity must be examined in dealing with  $UBV$  photometric reductions because the  $U$  passband, centred on  $\sim 3600 \text{ \AA}$ , extends partially across the discontinuity. Variations in its strength shift the effective wavelength of the  $U$  filter. The greater the discontinuity, the larger the effective shift (Moffat and Vogt 1977). That can result in a spectral type dependence for the extinction coefficient used to reduce the instrumental  $U$  data to the standard system since the extinction coefficient is tied to the colour term in the reduction equation. In essence, one simple linear relation to reduce instrumental photometric data for stars of varying spectral types is not sufficient. A more rigorous treatment, using spectral type as an independent variable as well as colour, is necessary. Unfortunately the spectral types of stars are quite often not known beforehand, and assumptions have to be made in order to conduct such a treatment.

The effect of the Balmer discontinuity may be further complicated by a mismatch of the actual  $UBV$  passbands used in comparison with the standard  $UBV$  passbands defined by Johnson and Morgan in 1953. The  $UBV$

photometric system was originally defined as measured by a specific photomultiplier tube, namely the RCA type 1P21, through now-standard *UBV* filters (Johnson 1963). Any observations with a different instrument, such as a CCD, run the risk of a mismatch with the original system. With the varieties of technical modifications designed to enhance sensitivities in various regions of wavelength, CCD response functions may not even be consistent within specific models.

A good way to determine the extent of error in *U* data is to compare correctly reduced CCD photometry, observed with one filter and detector combination, with reliable photoelectric photometry, assumed to be determined under conditions well-matched with the standard *UBV* instrumentation. A discussion of standard systems that have been used in photoelectric photometry, and problems lying therein, has been presented by Bessell (1990). Without an opportunity to study each set of published photoelectric photometry in detail, the effects of possible mismatches have been assumed to be negligible.

The comparison of CCD photometry with photoelectric photometry is meant to quantify any correction needed to transform CCD magnitudes to standard magnitudes as a function of spectral type. Thus, determinations of spectral type for comparison stars are also necessary. Often, spectroscopic data are not available for the number of stars necessary for a comparison of this type. Approximate photometric spectral types, based on dereddened colour indices of stars in open clusters, are a source of such data and have been used in the following analysis.

A more rigorous treatment of the problem of standardizing ultraviolet

let passbands in conjunction with CCDs has been done by Straižys and Lazauskaitė (1995). The authors numerically convolved the response function of the detector, telescope and filter combination, the energy distribution function describing the spectra of different type stars, and the transmission function of both the atmosphere, and interstellar dust and compared the resultant function for a CCD detector system with that of the standard *UBV* system. Their results indicate that, for several detector systems, synthesized ultraviolet colour indices vary from those synthesized using standard system parameters by up to 0.1 magnitude. The non-linear effect for stars with large Balmer discontinuity is evident in their Figs. 7 – 9.

While a study of synthesized colour indices for such a detector and filter combination would be a useful technique for any type of calibration, such an involved numerical study was beyond the constraints of this thesis. Instead, an empirical method of calibration was chosen. A set of well-reduced *UBV* photometric data for our detector/filter system was compiled, and compared with well-reduced photoelectric data for the same stars. The largest source of CCD data was an extensive study done by Shelton (1996). The data reduced for the preparation of this thesis were also used.

For stars studied by Shelton, existing photoelectric data were used in the regions of NGC 6231 (Garrison and Schild 1979; Schild *et al.* 1969) Bochum 13 (Moffat and Vogt 1975) and Hogg 22 (Forbes and Short 1996), and for stars studied photometrically by Schild *et al.* (1983). The data used in the preparation of this thesis were compared with photoelectric photometry by Havlen and Moffat (1977) and Pedreros (unpublished).

As the effect normally depends on spectral type, spectral types were

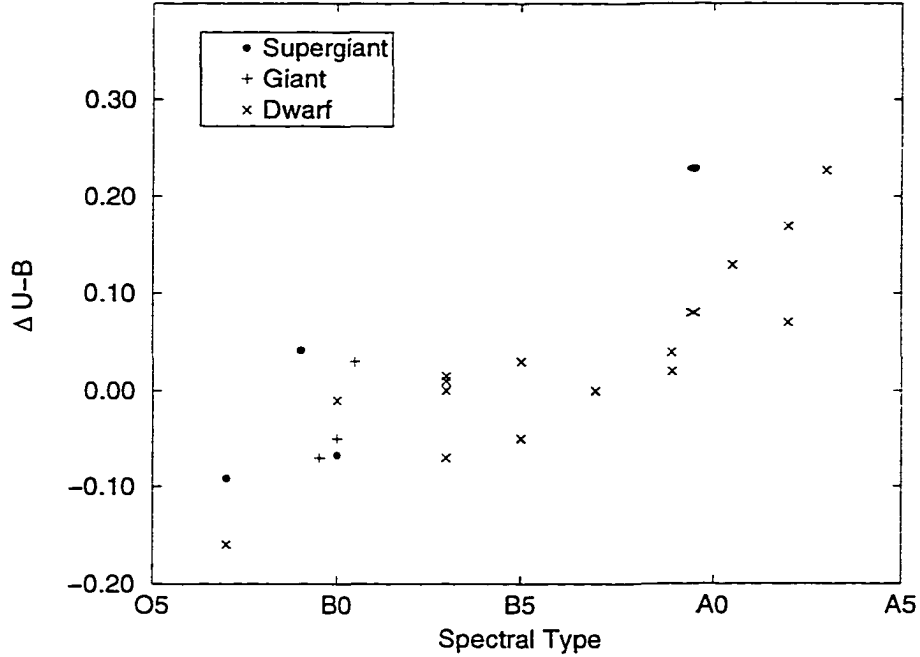


Figure 3.1: Discrepancy in  $U-B$  data ( $\Delta(U-B) = (U-B)_{p.e.} - (U-B)_{ccd}$ ) as a function of spectral type

taken, where possible, from Garrison *et al.* (1977). Spectroscopically determined spectral types were also adopted as listed in the aforementioned references, and references therein. When no spectroscopic data were given, approximate spectral types were adopted by dereddening stars to the main sequence, as shown on colour-colour diagrams in the appropriate references. The data as a function of spectral type are seen in Figure 3.1.

The data suggest that a small constant correction in  $U-B$  may be appropriate for stars earlier than spectral type B9. Later than that, a linear correction up to spectral types A2-A3 seems appropriate. Later than spectral

type A3 there are no reliable data. Since the effect of the Balmer discontinuity is greatest at spectral types A2-A3 and then decreases for later-type stars, a symmetrical correction was adopted, to be used for stars as late as spectral type A6.

No data are available for stars later than spectral type A3, so it is impossible to suggest what the effects for the later-type stars are. Therefore, no corrections were adopted other than those given above. The procedure may result in incorrect  $U-B$  colours for later-type stars, but nothing further could have been done.

The effect on A-type stars may be seen clearly in at least two sets of observations performed previously at UTSO, the  $UBVRI$  observations of the open cluster NGC 5606 by Vázquez *et al.* (1994) and the  $UBVRI$  observations of the open cluster Cr 272 by Vázquez *et al.* (1997). Figure 3 of Vázquez *et al.* (1994) shows a colour-colour diagram with a well-defined reddened intrinsic relation with little differential reddening. Yet, six data points lie above the intrinsic relation in the mid A-type region. Figure 4 of Vázquez *et al.* (1997) shows a similar morphology, with approximately ten of their “probable members” lying above a reddened intrinsic relation which fits well the O and B type cluster members. If a spectral type dependent correction in  $U-B$  had been applied to the points as prescribed above, the stars could be dereddened as mid A-type stars with comparable reddenings to that of the cluster. As it was, the stars were dereddened as late B-type stars with anomalous reddenings. It must be noted that the systematic errors in  $U-B$  as outlined would be difficult to recognize clearly in a cluster with differential reddening, as may be seen in other studies using UTSO (*e.g.*, Vázquez *et al.*

1995).

In the case of HM 1, the relation between  $\Delta U$  and  $(B-V)_{\text{std}}$  was obviously not linear over the entire range of  $B-V$  values. The relation between  $\Delta U$  and  $(B-V)_{\text{std}}$  is linear, however, for the stars with  $B-V > 1.4$ , *i.e.*, the highly reddened OB cluster members. Since the purpose of this study is to provide photometry for cluster stars, only those stars in the field of HM 1 which were obvious highly reddened OB cluster members were assigned standardized  $U$  values. The calibration was done as prescribed in Equation 3.1, but with only the cluster members as comparison stars. Unfortunately, several stars imaged in the north-east and south-east frames have been identified as members based upon their approximate colours, but precise  $U$  values could not be determined because of a lack of standards in those regions.

All identified stars in the HM 1 region are labeled on Figure 3.2. Stars 13 and 46 are not visible on the finder chart as they are, respectively, very near stars 3 and 1. Short lines have been drawn pointing to their approximate positions. All identified stars in the Carina region are labeled on Figure 3.3 and the inset Figure 3.4. The inset has been included to unambiguously identify the stars in the new cluster region, and has been created from a CCD image taken by the author.

The uncertainty in the photometry is quantified by comparing stars which have magnitudes derived from different exposures. A plot of standard deviation in magnitude between exposures for each of  $V$ ,  $B$ , and  $U$  is plotted in Figure 3.5 for HM 1 data and Figure 3.6 for Carina region data. For HM 1 region observations, the uncertainties are estimated to be  $\Delta V = \pm 0^{\text{m}}01$  up to  $V = 14.0$ , increasing to  $\Delta V = \pm 0^{\text{m}}04$  at  $V = 16$ ,  $\Delta B = \pm 0^{\text{m}}01$  up to

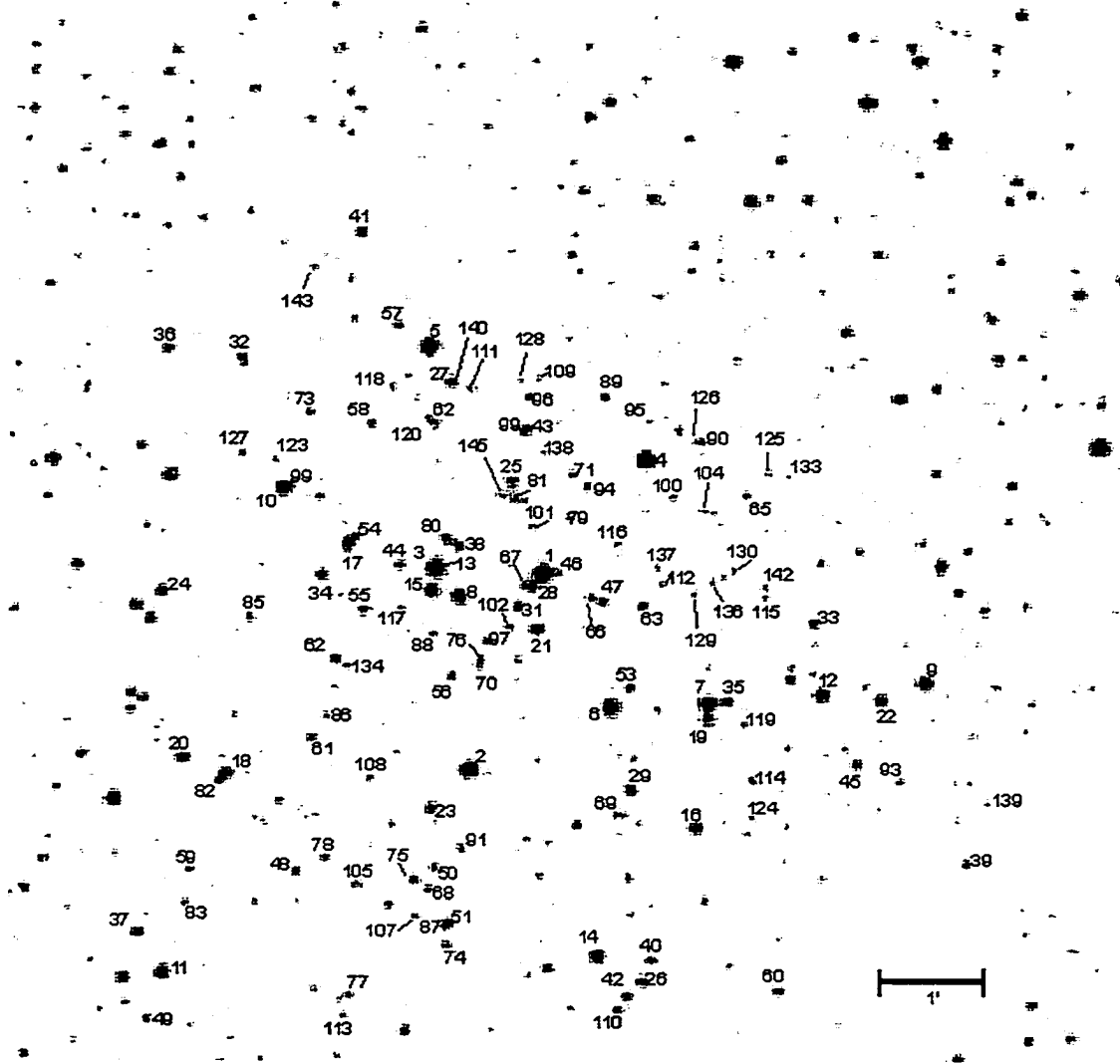


Figure 3.2: HM 1 region finder chart. North is up and east is to the left.

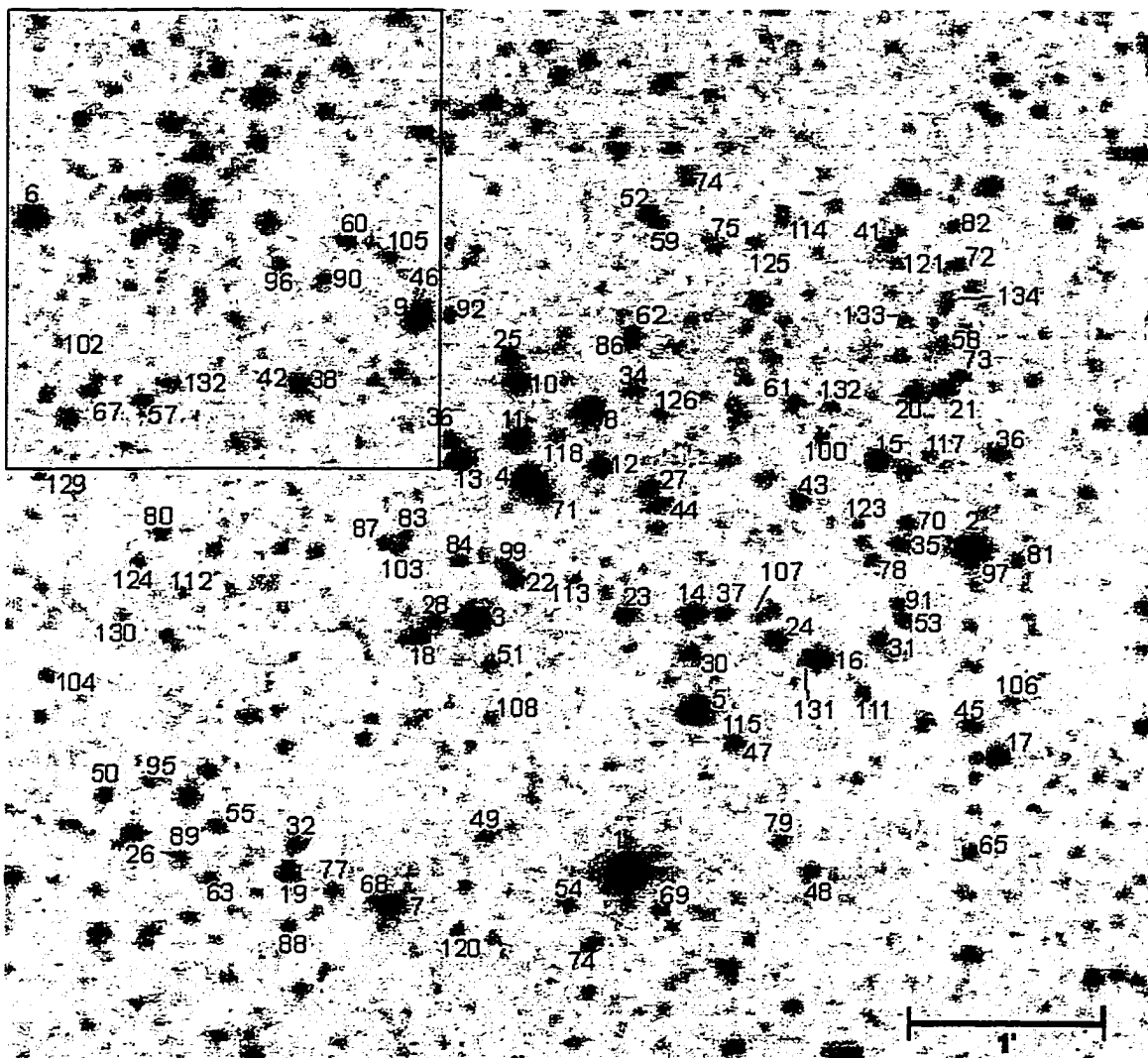


Figure 3.3: Carina region finder chart. North is up and east is to the left. The inset is labelled in detail on Figure 3.4.

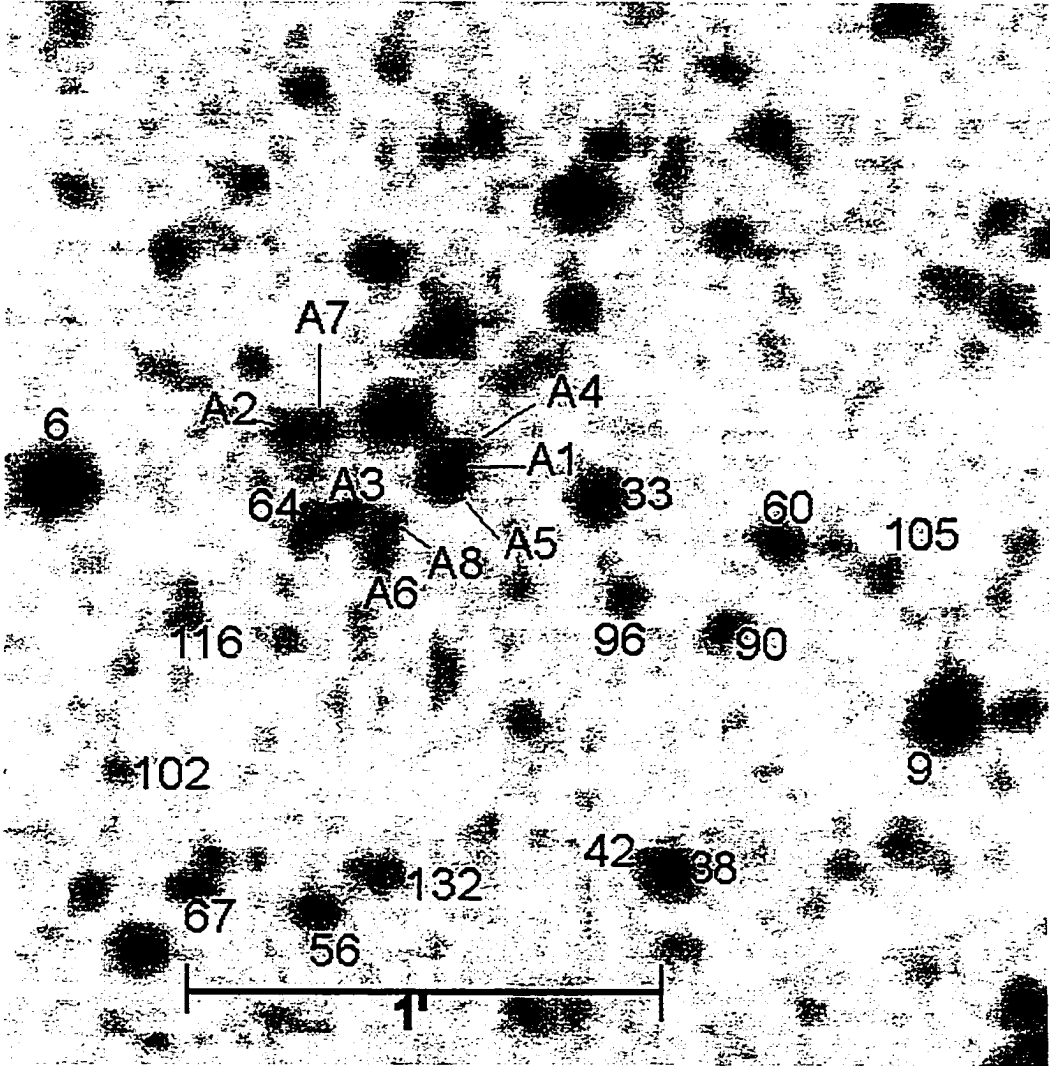


Figure 3.4: Carina region finder chart inset. North is up and east is to the left.

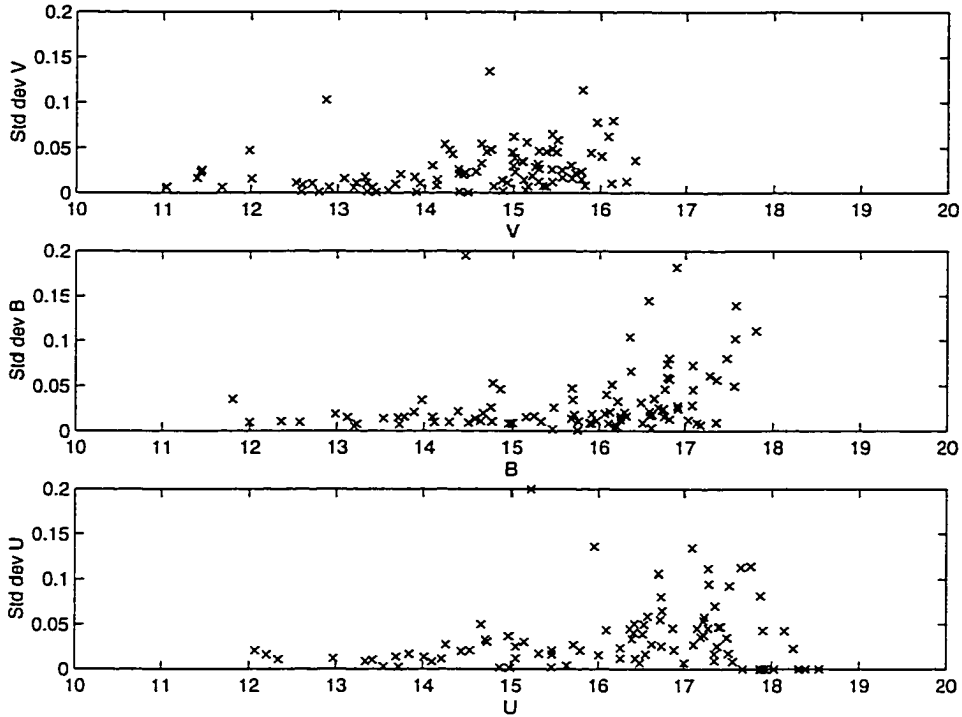


Figure 3.5: Standard deviation in magnitude between exposures in  $V$ ,  $B$ , and  $U$  for the HM 1 field

$B = 15.5$ , increasing to  $\Delta B = \pm 0^m04$  to  $B = 17$ , and  $\Delta U = \pm 0^m015$  up to  $U = 15.0$ , increasing to  $\Delta U = \pm 0^m05$  at  $U = 17.5$ . For Carina region observations, the uncertainties are estimated to be  $\Delta V = \pm 0^m015$  up to  $V = 14.0$ , increasing to  $\Delta V = \pm 0^m01$  at  $V = 16$ ,  $\Delta B = \pm 0^m01$  up to  $B = 15.5$ , increasing to  $\Delta B = \pm 0^m04$  to  $B = 17$ , and  $\Delta U = \pm 0^m01$  up to  $U = 15.0$ , increasing to  $\Delta U = \pm 0^m05$  at  $U = 17.5$ . The uncertainties in the colours  $B-V$  and  $U-B$  will thus be of the order  $\pm^m01$  for the brightest stars and up to  $\pm 0^m08$  for the faintest stars.

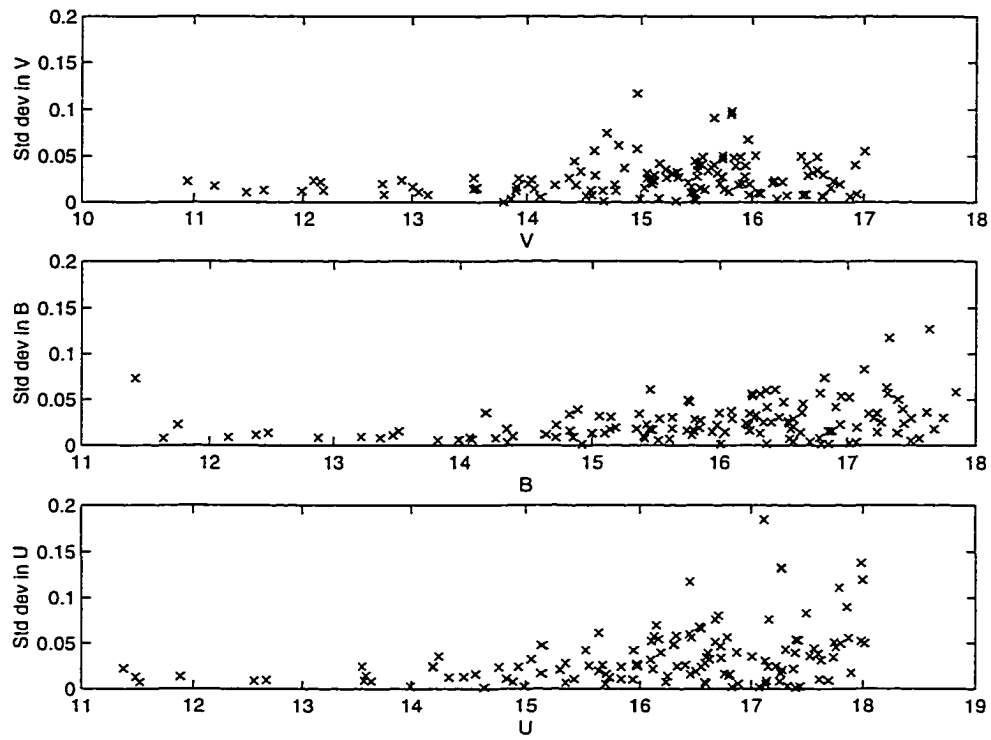


Figure 3.6: Standard deviation in magnitude between exposures in  $V$ ,  $B$ , and  $U$  for the Carina field

# Chapter 4

## HM 1

### 4.1 Extinction

Analysis of the clusters began with an examination of the extinction in the regions of study. The colour excess indices  $E_{B-V}$  and  $E_{U-B}$  are defined as

$$E_{B-V} = (B-V) - (B-V)_o \quad (4.1)$$

and

$$E_{U-B} = (U-B) - (U-B)_o, \quad (4.2)$$

where  $(B-V)_o$  and  $(U-B)_o$  are the intrinsic colours of the stars. The relationship between colour excesses is usually described by an equation of the form,

$$\frac{E_{U-B}}{E_{B-V}} = X + Y \cdot E_{B-V}, \quad (4.3)$$

where  $X$  is the reddening slope and  $Y$  is a curvature term. For a small range in  $E_{B-V}$ , the relationship between  $E_{U-B}$  and  $E_{B-V}$  will be approximately linear with a constant slope.

The reddening slope for each field of study was investigated by searching the literature for photometric and spectral classification data for stars near the regions of study. OB stars studied and numbered by Klare and Szeidl (1966) have published photometry by Klare and Neckel (1977) and Schild *et al.* (1983) and spectral classifications by Garrison *et al.* (1977). Spectral types and luminosity classes are translated into intrinsic colours for each star as prescribed by Turner (private communication). The photometric data sets

were adjusted to the standard *UBV* system according to Drilling (1991) and then averaged.

In each case stars were selected that were within  $\sim 1^{\circ}5$  in both  $l$  and  $b$  of the centre of the field. Stars designated “n” and/or “e” (denoting blurring from rapid rotation or the presence of emission, respectively) were initially included, but several such stars had colour excesses that did not seem to fall along the general trend of the others. Since precise spectral classification of stars with blurred spectra may be difficult and some emission-line stars have intrinsic ultraviolet excesses, the stars with the “n” and “e” designations were excluded as a group.

Eight stars near HM 1 were initially chosen to examine the reddening. The chosen stars were not as highly reddened as the stars in the cluster itself, and so a simple linear relation based on only slightly reddened stars would have been inappropriate, assuming a non-negligible curvature term in Equation 4.3. As such, the reddening relation was determined using spectral types of cluster stars. Havlen and Moffat (1977) published reproductions of spectra for four stars in the cluster. Those spectra were examined by Turner and Forbes (unpublished) for the purpose of confirming the spectral types. The spectral types, inferred intrinsic colours and associated colour excesses are summarized in Table 3. The mean value of  $E_{U-B}/E_{B-V} = 0.80$  was adopted for the region. Also included in Table 3 are typical absolute magnitudes for stars of the given spectral types (Turner 1980). The uncertainty in the exact classification of star number 12 prohibits an accurate estimate of its absolute magnitude.

Star	Sp. Type	$(B-V)_o$	$(U-B)_o$	$E_{B-V}$	$E_{U-B}$	$E_{U-B}/E_{B-V}$	$M_V$
3	O4 If+	-0.33	-1.16	1.88	1.51	0.80	-7.0
5	O5 If+	-0.33	-1.16	1.88	1.48	0.79	-7.0
8	O8 Ib(f)	-0.31	-1.15	1.89	1.50	0.79	-6.2
12	O8 I:	-0.31	-1.15	1.82	1.50	0.82	

Table 3: Spectral types and inferred intrinsic colours, absolute magnitudes and colour excesses for stars in HM 1

## 4.2 Star Counts

In order to measure the angular size of an open cluster and to estimate the number of cluster members, star counts may be performed in a cluster region. A set of adjacent, equal-area parallel strips are drawn to cover the cluster region. Stars are counted in each strip and the peak in star density in the chosen direction is located. The procedure is repeated at least once, but in different directions than the first set, in order to locate the point which is the peak in star density. The peak is assumed to be coincident with the centre of the roughly circular open cluster. Counts are then performed by constructing annuli of increasing radius centred on the adopted cluster centre. Stars are counted in each annulus and the number of stars, normalized by the area of the annulus, plotted against distance from the cluster centre. Such a plot may be used to measure the cluster radius, after which the star density remains constant, and to estimate the number of stars within the cluster radius.

Star counts performed in this manner by Havlen and Moffat have not been redone for this study. The value of an excess of  $42 \pm 14$  stars above mean field star density inside the cluster radius of  $4'$  was adopted from their study.

### 4.3 Colour-colour diagram

A colour-colour diagram (CCD) for an open cluster is a plot of  $U - B$  vs.  $B - V$  for stars in the cluster region. A CCD is usually drawn with the unreddened or intrinsic colour-colour relation for main sequence stars indicated. A CCD may be used as a preliminary discriminator between members and non-members of a cluster, as data corresponding to most members will be scattered about a relation shifted by some mean colour excess,  $E_{B-V}$ , along a reddening line of slope  $X$  as defined in Equation 4.3.

A point thought to correspond to a cluster member may be “dereddened” to the main sequence by finding the intersection of the intrinsic main sequence relation with a line of slope  $X$  that passes through the point. There may be zero, one, two, or three dereddening solutions for any given data point. Cases where there are unique solutions are used to estimate the mean colour excess as well as to outline variations of colour excess for cluster members on the sky. In a case where there are two or three possible solutions, the “correct” dereddening solution will be one that results in a colour excess that fits the general trend of colour excesses for nearby cluster members on the sky, as well as an intrinsic colour,  $(B - V)_o$ , for the star that fits its magnitude rank in the cluster.

Dereddening to the main sequence is done under the assumption that apparent cluster members are main sequence objects, which is not always the case. The brightest and presumably most evolved members of a young to intermediate age open cluster will not necessarily be main sequence stars. If, for several of the brighter stars in the field, dereddening does not provide colour excesses that fit the estimated mean reddening, they should be

assigned colour excesses based upon colour excesses for nearby cluster members. The stars should then be examined to see if such an assignment resulted in intrinsic colours for the stars that fit with an evolved star of that magnitude rank in the cluster.

The colour-colour diagram for HM 1 in Figure 4.1 shows a relatively small number of highly reddened ( $E_{B-V} \approx 1.9$ ) OB members with a large number of less-reddened foreground stars. As all candidate members could be dereddened uniquely to the OB section of the intrinsic two-colour relation,  $U-B$  values obtained by the calibration using only cluster members as standards did not need corrections for systematic errors. Non-member field stars, however, may have uncorrected systematic errors in  $U-B$ , since no information about their spectral types is available. Photometric data for stars in the HM 1 region are tabulated in Appendix A.

$(B-V)_o$  colours for all members excluding the WR stars were assigned according to the intersection of the two lines,

$$(U-B)_o = 3.758 \cdot (B-V)_o + 0.04, \quad (4.4)$$

which is the upper part of the intrinsic colour-colour relation for OB stars, and

$$(U-B) - (U-B)_o = 0.80 \cdot [(B-V) - (B-V)_o] \quad (4.5)$$

where  $U-B$  and  $B-V$  were the colours specific to each star.  $(B-V)_o$  values and the associated colour excess values are included in Appendix A.

#### 4.4 Reddening

The reddening map for candidate members of HM 1, Figure 4.2, shows variable reddening across the field as also found by Havlen and Moffat (1977).

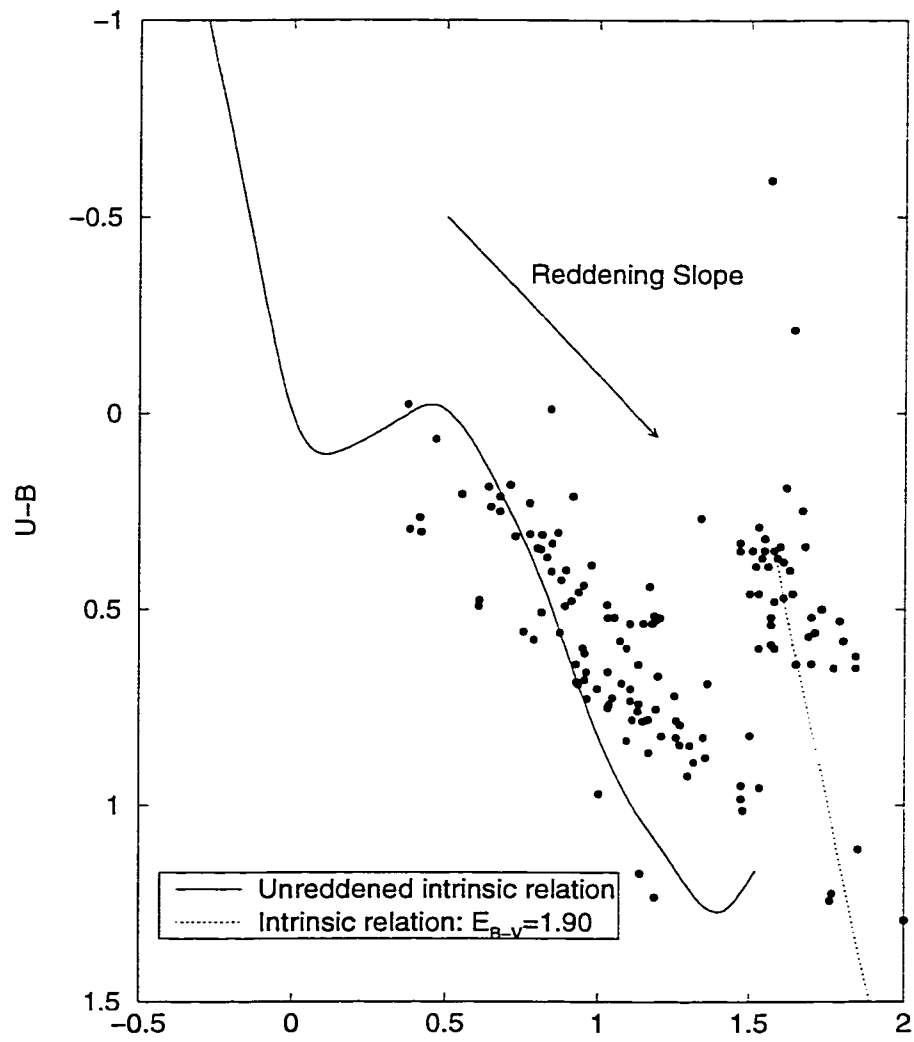


Figure 4.1: Colour-colour diagram for HM 1 region

Colour excesses for the WR stars, identified as stars 1 and 7, were adopted based on the colour excesses of nearby stars. The five stars nearest star number 7 have colour excesses  $E_{B-V} = 2.03, 2.00, 2.11, 1.82$  and  $1.95$  for a mean colour excess  $\langle E_{B-V} \rangle = 1.98 \pm 0.05$  (s.e.). The twelve stars nearest star number 1, excluding star number 46, have colour excesses  $E_{B-V} = 1.86, 1.80, 2.13, 1.83, 1.86, 1.77, 1.89, 1.85, 1.93, 1.94, 1.96, 1.82, 1.82$ , for a mean colour excess  $\langle E_{B-V} \rangle = 1.88 \pm 0.03$  (s.e.). Star number 46 was excluded from the calculation of a colour excess for the WR star because it is very near the much brighter star number 1, and thus its photometry is more uncertain. Reliable colour excesses for cluster stars range from  $E_{B-V} = 1.75$  to  $2.14$  and produce a mean of  $\langle E_{B-V} \rangle = 1.92$ .

## 4.5 Variable-Extinction Diagram

The relation

$$V - M_V = R \cdot E_{B-V} + V_o - M_V \quad (4.6)$$

where  $R = A_V/E_{B-V}$ , the ratio of total to selective absorption, may be extrapolated to  $E_{B-V} = 0$  to determine the true cluster distance modulus. The use of the “lower envelope” of the variable extinction data has been described by Turner (1976a, 1976b). In general,  $R$  has been found to be approximately equal to 3, with systematic variations found in different regions of the Galaxy. Recently, the dependence of  $R$  on reddening slope  $E_{U-B}/E_{B-V}$  has been investigated by Turner (1996) and the relation

$$R = 5.240 - 3.022 \cdot E_{U-B}/E_{B-V} \quad (4.7)$$

has been derived empirically for local dust clouds using results for well-studied fields.

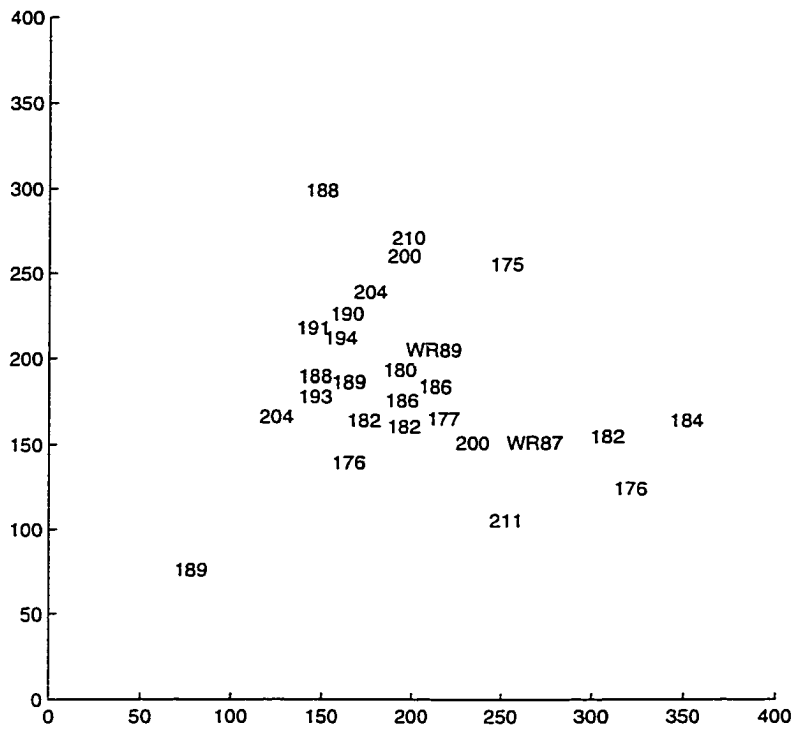


Figure 4.2: Reddening Map of HM 1 based upon colour excesses  $E_{B-V}$ . The locations of stars WR 87 and WR 89 are indicated. The origin is the southeast corner of the SE frame as shown on Figure 2.1. Axis units are  $0^m02$ .

Absolute magnitudes and colour excesses for three stars classified by Turner and Forbes, as listed in Table 3, have been used in the variable extinction analysis. The variable extinction diagram for candidate members of HM 1, Figure 4.3, exhibits a spread in  $V-M_V$  values typical of open clusters. The data seem to deviate from the expected relation  $V-M_V = R \cdot E_{B-V}$  with  $R \approx 3$ , and are somewhat suggestive of a larger slope. Random scatter in the  $U-B$  and  $B-V$  data may have affected the dereddening, as illustrated by Turner (1976a). When a fit was made of a line of slope  $R = 2.8$ , derived from Equation 4.7, through the lower envelope of the data, a distance modulus  $V_o - M_V = 12.9 \pm 0.2$  was derived for HM 1, where the uncertainty was estimated by keeping a reasonable fit to the lower envelope data. Such a relation was obtained from the data after omitting the two points with  $V-M_V > 19$ , since one is near the photometric reliability limit and the other is quite highly reddened and likely a background object. The points based on spectroscopic data are located in the same lower envelope.

Using only the three stars with colour excesses and absolute magnitudes based upon spectral classification, the measured distance moduli are  $V_o - M_V = 13.2, 13.4$  and  $13.4$  for a mean distance  $\langle V_o - M_V \rangle = 13.3 \pm 0.1$  (s.e.). Calculated values of  $V_o - M_V$  for several other cluster members do not agree well with this estimate, or in some cases with each other. It may be that for several of the brighter objects, the assumption that they are main sequence stars is incorrect. In that case, dereddening to the main sequence results in incorrect estimates of both intrinsic colour and absolute magnitude. It may also be that the adopted reddening slope is incorrect, but the good agreement between the estimates of the reddening slope made by examining the stars

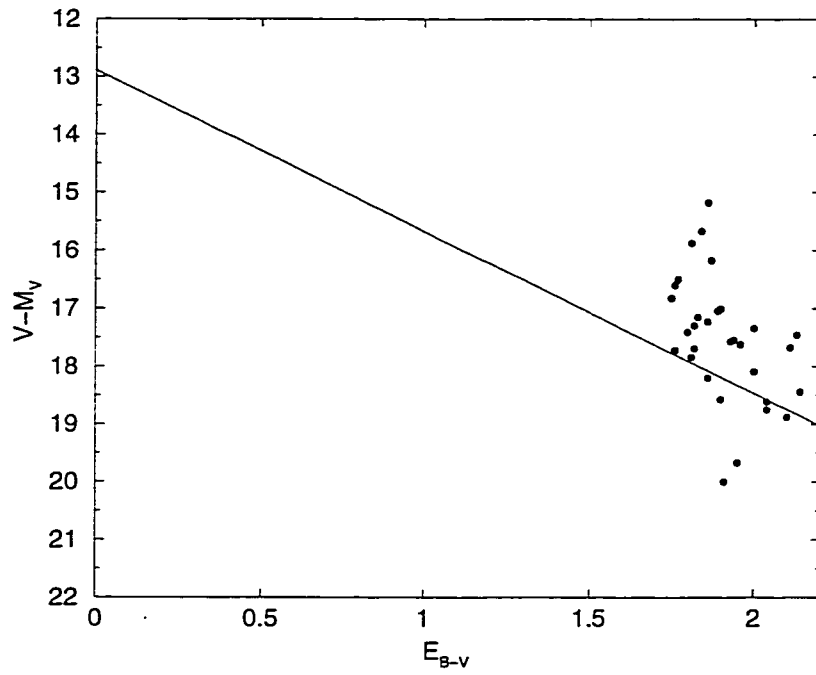


Figure 4.3: Variable extinction diagram for HM 1

with published spectra would seem to imply that the reddening slope is correct. The uncertainties in the photometric data may also contribute to the disparate values of  $V_o - M_V$ , especially since even small errors in photometric data may cause the dereddened colours and thus the absolute magnitudes to be very uncertain. Finally, the binarity and rotation expected to be present in a sample of members of a young open cluster will contribute to errors in estimates of distance modulus.

Under the assumption that estimates of  $V_o - M_V$  for the brightest cluster members are most affected by systematic errors introduced in dereddening data with random errors, as illustrated by Turner (1976a), as well as possible evolution off the main sequence, they have been excluded in a more comprehensive measure of the cluster distance. Among the faintest cluster members, only the stars with the largest distance modulus measures have been included, as the others are assumed to be binary and affected by rapid rotation. Including only stars numbered 3, 5, 8, 55, 56, 63, 80, 96, 100, 102, 103, 135 and 145, the mean distance is measured to be  $\langle V_o - M_V \rangle = 13.19 \pm 0.16$  (s.e.).

## 4.6 Colour-magnitude diagram

A colour-magnitude diagram (CMD) of an open cluster is a plot of colour, *e.g.*,  $(B - V)_o$ , *vs.* magnitude, *e.g.*,  $V_o$ , for probable cluster members. The CMD for members of HM 1 is similar to that of an extremely young star cluster. Unfortunately, the uncertainty of the absolute magnitude-intrinsic colour relation for the hottest stars does not allow for an accurate measure of the main sequence turn-off point (MSTO). With an estimated MSTO of  $(B - V)_o < -0.32$ , the cluster must have an age  $\log t < 6.5$  (Turner, private

Star	HM #	$V$	$B-V$	$U-B$	$E_{B-V}$	$(B-V)_o$	$V_o$	$V_o - M_V$	Comment
1	1	11.04	1.52	0.39	1.88	-0.31	5.92		WR 89
3	2	11.43	1.55	0.35	1.88	-0.33	6.17	13.2	O4 If+
5	6	11.68	1.55	0.32	1.88	-0.33	6.42	13.4	O5 If+
7	3	12.01	1.69	0.57	1.98	-0.34	6.33		WR 87
8	8	12.51	1.58	0.35	1.89	-0.31	7.22	13.4	O8 Ib(f)
9	12	12.57	1.54	0.37	1.84	-0.30	7.35		
12	13	12.78	1.51	0.35	1.82	-0.31	7.68		O8 I:
13		12.86	1.62	0.19	2.01	-0.39	7.18		
15	9	13.07	1.61	0.38	1.93	-0.32	7.61	12.11	
16	16	13.18	1.79	0.53	2.11	-0.32	7.21	11.71	
21	18	13.40	1.47	0.33	1.77	-0.30	8.39	11.49	
28	10	13.94	1.53	0.29	1.86	-0.33	8.68		
31	19	14.13	1.56	0.39	1.86	-0.30	8.86	11.96	
38		14.44	1.64	0.48	1.94	-0.30	8.94	12.04	
43		14.64	1.71	0.56	2.00	-0.29	8.99	11.69	
45		14.70	1.50	0.46	1.76	-0.26	9.71	11.61	
46		14.73	1.67	0.25	2.05	-0.38	8.93		
47		14.76	1.84	0.65	2.13	-0.29	8.73	11.43	
53		14.99	1.70	0.52	2.00	-0.30	9.34	12.44	
55		15.00	1.73	0.50	2.04	-0.31	9.22	12.97	
56	23	15.02	1.47	0.35	1.76	-0.29	10.03	12.73	
63		15.17	1.63	0.40	1.95	-0.32	9.65	14.05	
64		15.22	1.68	0.34	2.03	-0.35	9.47		
66		15.25	1.57	0.52	1.83	-0.26	10.06	11.96	
67		15.28	1.53	0.46	1.80	-0.27	10.18	12.31	
71		15.34	1.84	0.62	2.14	-0.30	9.28	12.38	
80		15.50	1.59	0.37	1.91	-0.32	10.10	14.60	
83		15.52	1.65	0.64	1.89	-0.24	10.16	11.68	
90		15.65	1.53	0.60	1.75	-0.22	10.68	11.85	
94		15.72	1.70	0.64	1.96	-0.26	10.18	12.08	
96		15.78	1.80	0.58	2.10	-0.30	9.82	12.92	
97		15.78	1.58	0.60	1.82	-0.24	10.64	12.16	
100		15.80	1.58	0.48	1.86	-0.28	10.54	12.94	
102		15.82	1.57	0.54	1.82	-0.26	10.65	12.55	
103		15.87	1.61	0.47	1.90	-0.29	10.49	13.19	
135		16.32	1.57	0.59	1.81	-0.24	11.20	12.72	
145		16.48	1.77	0.65	2.04	-0.27	10.70	12.83	

Table 4: Photometry for members of HM 1 used to estimate  $V_o - M_V$ .

communication). An additional estimate of age could be made by locating stars near the main sequence turn-on point, but given the faintness of such objects, no estimate could be made confidently. Havlen and Moffat noted the similarity of their  $V_o$  vs.  $(U - B)_o$  diagram to those of two young OB associations – Ori OB1d and Per OB2 – and estimate an age of less than  $10^6$  years, which is reasonable in view of the CMD presented here.

The uncertainty in fitting the main sequence of such a young cluster is illustrated in Figure 4.4 by the inclusion of ZAMS lines for two distances. The ZAMS line for  $V_o - M_V = 13.19$ , the distance modulus obtained in Section 4.5, is a reasonable fit to the lower portion of the data, but the uncertainty in the absolute magnitude-intrinsic colour relation for the earliest stars makes that fit uncertain. A ZAMS line for  $V_o - M_V = 12.0$  also gives a fairly reasonable fit to the data, although in view of how binarity and rapid rotation of member stars can create systematic scatter above the main sequence as well as the possible evolution of the brightest stars,  $V_o - M_V = 12.0$  is likely to be a lower bound for the true distance modulus. Based upon the distance modulus obtained from the variable extinction analysis and the likelihood that the poor fit to the main sequence is caused by binarity and rotation, we adopted here a distance modulus for HM 1 of  $V_o - M_V = 13.19 \pm 0.16$ . It is larger than the distance modulus of  $V_o - M_V = 12.3 \pm 0.3$  derived by Havlen and Moffat (1977).

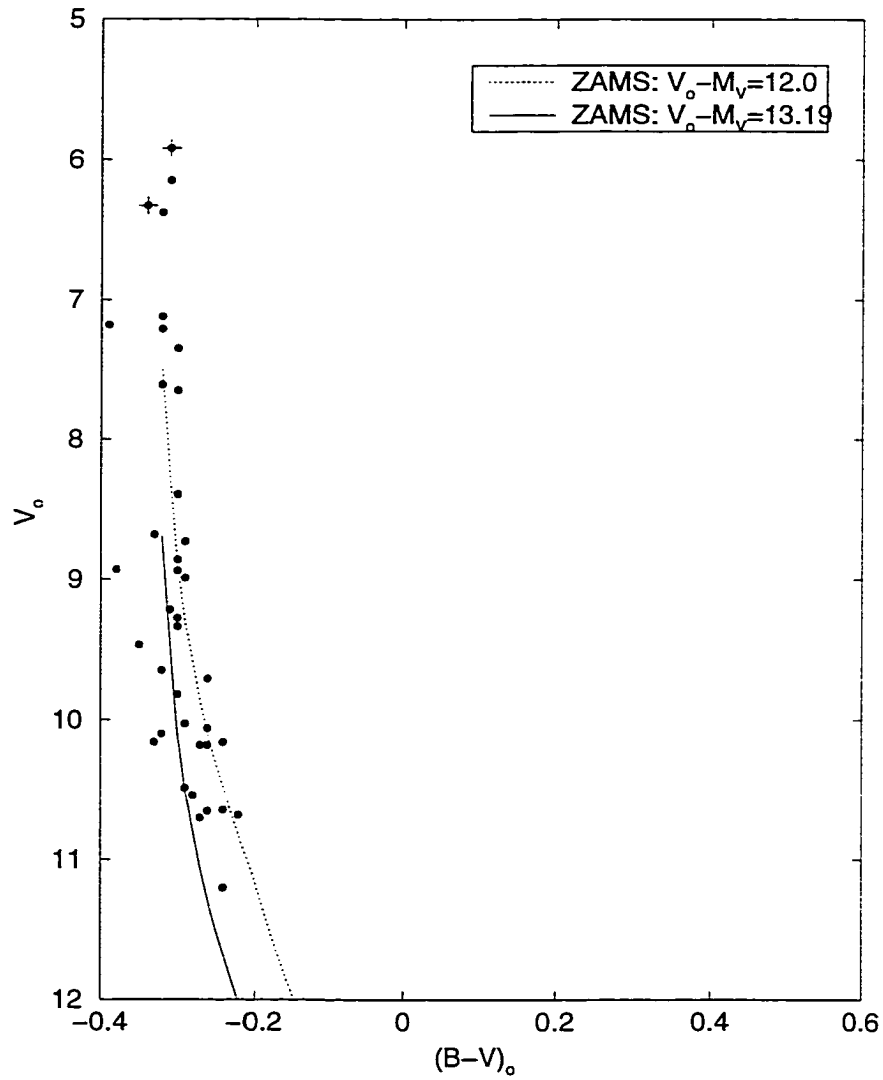


Figure 4.4: Colour Magnitude Diagram for HM 1 stars. WR stars are indicated by crossed filled circles.

# Chapter 5

## Distant Cluster

### 5.1 Extinction

An analysis of the extinction in the region of the candidate open cluster was performed, but the results were not useful in the cluster analysis. The complications were similar to those occurring in the analysis of the extinction in the HM 1 region as outlined in Section 4.1; the apparent cluster members were much more highly reddened than the stars from the studies by Klare and Neckel (1977), Schild *et al.* (1983), and Garrison *et al.* (1977). Again, according to Equation 4.3, a relation based upon slightly reddened stars would not have been appropriate. Since there were no stars in the region with known colour excesses as large as those in the candidate cluster, the reddening slope was adopted according to the equation

$$\frac{E_{U-B}}{E_{B-V}} = 0.75 + 0.02 \cdot E_{B-V}, \quad (5.1)$$

as determined from past studies of the Carina region. It is necessary to point out that the relation in Equation 5.1 may not hold true for a cluster at a large distance, as will be indicated for the candidate open cluster. The relation does provide, however, the best estimate for the reddening slope available for this thesis.

### 5.2 Star Counts

Star counts could not be performed as outlined in Section 4.2 for the candidate cluster. As will be discussed in Section 5.3, only eight faint stars

within an area of approximately one square arcminute are identifiable as cluster members. Since the eight identified stars are very near the detection limit for the images, it may be presumed that they are the brightest cluster members. Without deeper imaging, star counts will be dominated by field stars and any derived stellar density peak or radius will not reflect cluster parameters.

### 5.3 Colour-colour diagram

The CCD for the region in Carina was plotted and analyzed as outlined in Section 4.3. In order to detect a young open cluster associated with the two WR stars, the CCD was examined for evidence of reddened OB stars, as they would be the brightest members of a WR open cluster other than the WR stars themselves. Nine stars were identified as possible main sequence OB stars with similar reddenings ( $E_{B-V} \approx 1.6$ ). They were stars numbered A3, A4, A5, A6, A7, A8, 12, 113 and 131 as marked on finding charts in Figures 3.3 and 3.4. On the finding charts, six of the points make up a group of faint stars near one another on the sky and near the two WR stars: A1 (WR 38) and A2 (WR 38a). As they were also highly reddened, a value of  $E_{U-B}/E_{B-V} = 0.78$  was adopted for their dereddening according to Equation 5.1, for a mean  $\langle E_{B-V} \rangle = 1.6$ . Photometric data for stars in the highly reddened group are included in Table 11 in Appendix B.

The apparent members were dereddened as main sequence O and B stars according to the procedure in Subsection 4.3, with the appropriate reddening slope given above. Unfortunately they are quite faint and as such, their photometric data may be somewhat unreliable. The three faintest cluster members have only one photometric measurement in each of  $U$ ,  $B$ , and  $V$ .

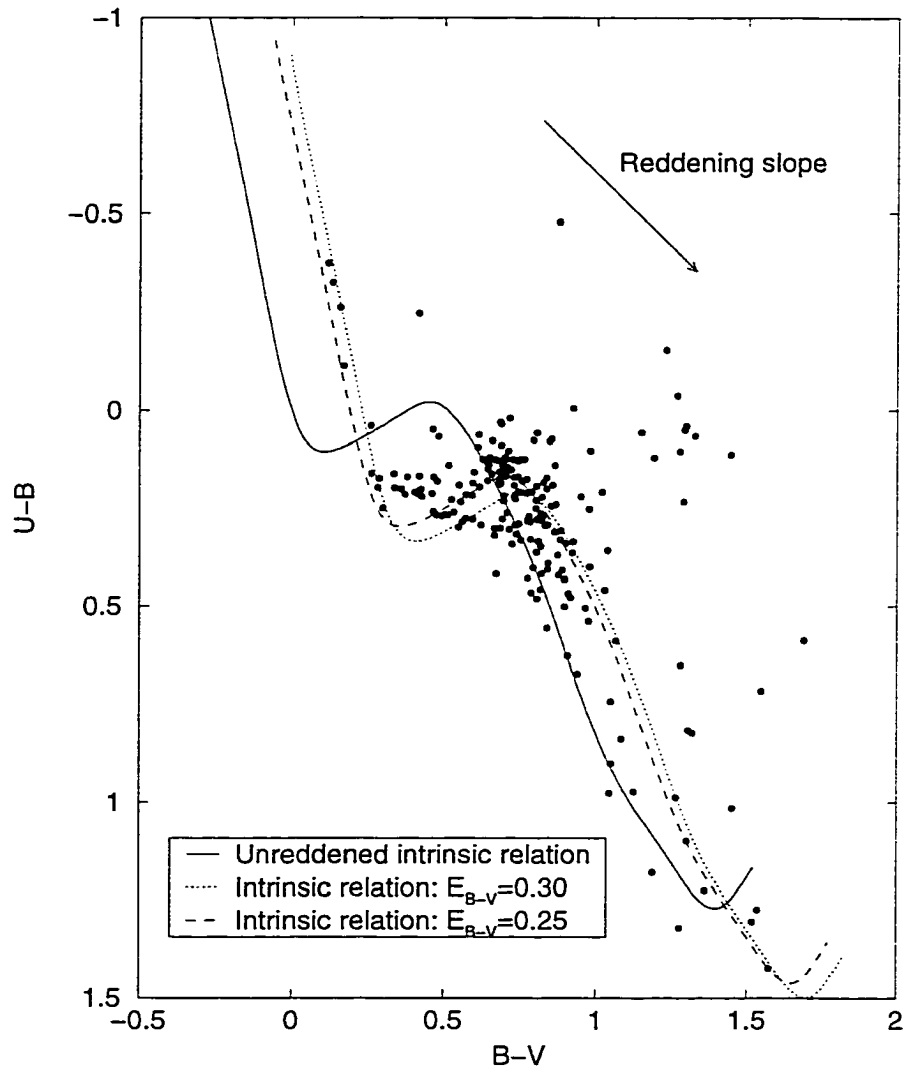


Figure 5.1: Uncorrected colour-colour diagram for the Carina region

Star number A5 is very near the brighter star number A1, which may have contributed to an error in the photometric data for it. As it stands, star number A5 may be dereddened to  $(B-V)_o = -0.39$ , which is inconsistent with its magnitude rank in the cluster.

According to IAU naming conventions, the open cluster is to be designated OCL 1104-610, based upon its apparent centre at  $\alpha = 11^{\text{h}}04^{\text{m}}$ ,  $\delta = -61^{\circ}00$ .

## 5.4 Variable-Extinction Diagram

A variable extinction diagram, as outlined in Section 4.5, could not be constructed for the new Carina cluster, given the uncertainty in the colour excess measures and the subsequent adoption of a single colour excess for all stars.  $V_o - M_V$  may be estimated for the four stars with  $(B-V)_o \geq -0.32$ : A3, A6, A7 and A8. Using measures of  $V_o - M_V$  for the brightest stars A3 and A6, we found the distance modulus to be  $\langle V_o - M_V \rangle = 15.5 \pm 0.2$  (s.e.). It must be noted that the distance is based primarily on an assumed value of  $R$ , the quality of which in this case cannot be evaluated. The true uncertainty in the distance moduli derived here must include the additional uncertainty in the value of  $R$ , which cannot be measured with the data in this thesis.

## 5.5 Colour-magnitude diagram

Data for the probable members of the distant cluster, as well as for WR 38 and WR 38a, are plotted on the CMD in Figure 5.3. As the dereddening process is prone to uncertainty given the faintness of the stars, a mean colour excess of  $\langle E_{B-V} \rangle = 1.6$  was adopted. It may underestimate the true reddening, but permits a reasonable determination of cluster parameters. The data for

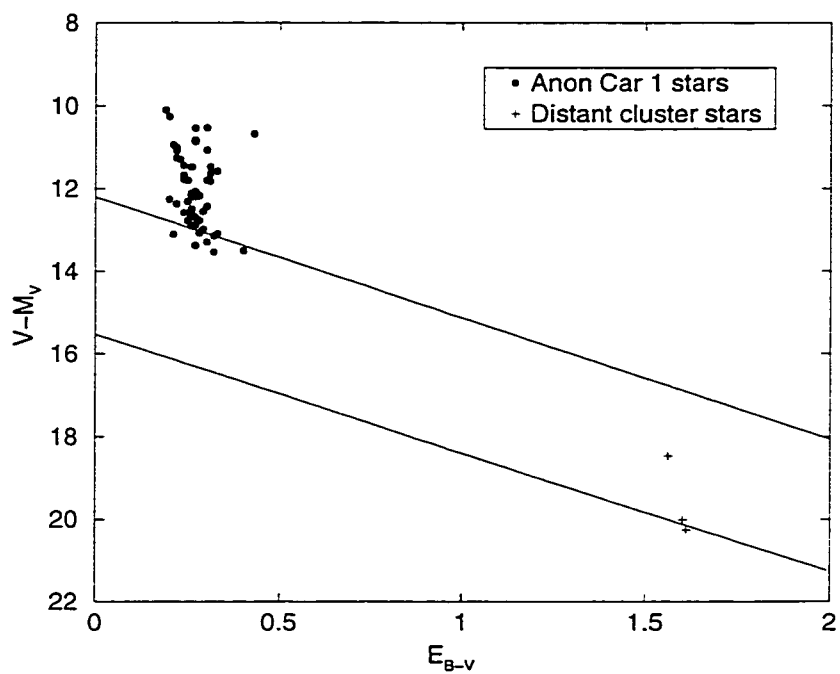


Figure 5.2: Variable extinction diagram for the Carina region

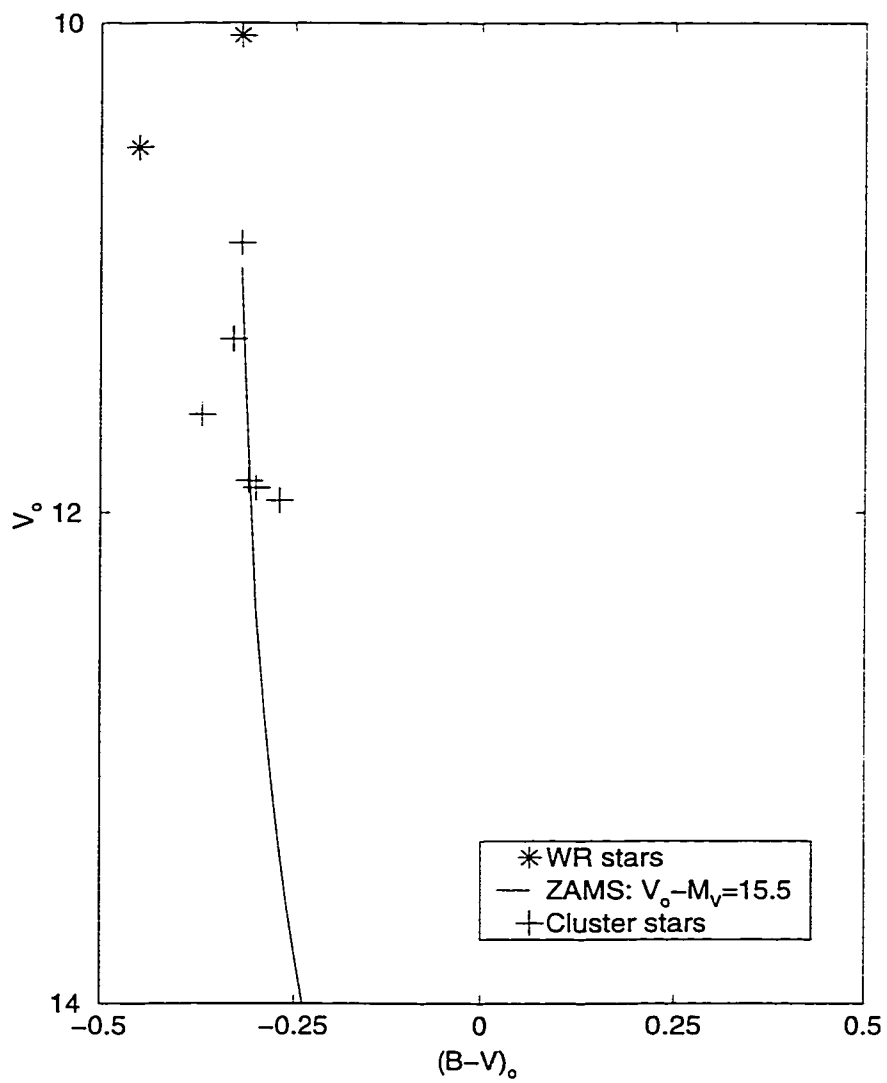


Figure 5.3: Colour Magnitude Diagram for Distant Cluster

the distant cluster members are rather uncertain, but a very young sequence of distant stars is obvious. The ZAMS relation is plotted for  $V_o - M_V = 15.5$ , which fits the data very well despite the fact that four of the stars have  $V > 16$ . From the fit of the ZAMS and the variable extinction analysis, the distant cluster is estimated to have a distance modulus  $V_o - M_V = 15.5 \pm 0.2$ , which implies that it is  $12.1 \pm_{1.1}^{1.2}$  kpc distant. The location of the MSTO is difficult to establish because of the uncertainty in the colour excess, but the main sequence appears to be populated to  $(B - V)_o \approx -0.32$ , which corresponds to an age of less than several Myr.

# Chapter 6

## The Wolf-Rayet Stars

### 6.1 Photometry and Intrinsic Parameters

The photometry of WR stars has been done predominantly in the narrow-band system,  $ubv$ , originated by Westerlund (1966) and developed by Smith (1968), with some data derived from synthetic filter photometry of stellar spectra approximating  $ubv$  photometry. The  $ubv$  photometric system was designed to minimize the contribution of the strong WR emission lines to the photometric magnitudes and colours. Relationships for transforming  $ubv$  data for normal stars to their equivalents on the Johnson  $UBV$  system have been derived by Turner (1981), and are given by

$$E_{B-V} = 1.21 \cdot E_{b-v}, \quad (6.1)$$

$$(B-V)_o = \text{Zero - point} + 1.30 \cdot (b-v)_o, \quad (6.2)$$

and

$$V = v - 0.033 - 0.365 \cdot (b-v). \quad (6.3)$$

A reddening law of slope  $R = 2.88$  implies an extinction in the narrowband system of  $A_v = 3.83 \cdot E_{b-v}$ , while  $R = 2.80$  implies  $A_v = 3.72 \cdot E_{b-v}$  and  $R = 2.94$  implies  $A_v = 3.91 \cdot E_{b-v}$ .

Applying the transformation to  $ubv$  data for WR stars will result in what may be termed “emission-free”  $UBV$  data. “Emission-free”  $UBV$  magnitudes and colours will not be equal to those measured by  $UBV$  photometry, due to the contamination from the emission lines. In the same way, the reverse transformation, from measured  $UBV$  to  $ubv$ , will not give accurate

*ubv* data. For the analysis of the individual WR stars, values of the distance modulus, colour excess and total extinction are used as transformed from the *UBV* system to the *ubv*, since they are derived from the *UBV* photometry of normal stars. *ubv* magnitudes and colours for the individual WR stars are adopted from previous photometric work in the narrow-band system only.

Many photometric studies of open clusters with WR members have been completed. Compilations and critiques of such studies, and their implications regarding intrinsic WR parameters, have been done by, *e.g.*, Lundström and Stenholm (1984b), van der Hucht *et al.* (1988), and Vacca and Torres-Dodgen (1990). The analyses have been used to derive a set of intrinsic parameters for WR stars based on their spectral types. Recently derived absolute magnitudes and colours for the relevant WR subtypes are listed in Table 5. Since there were no WC4 stars known to be in Galactic open clusters prior to this thesis, the values in Table 5 were extrapolated along the trend evident for WC5 to WC9 subtypes. Estimates of intrinsic parameters have also been made by observing WR stars in the Large Magellanic Cloud, but there are indications of systematic differences between galactic WR stars and those in the LMC (Smith *et al.* 1990).

Sp. Type	$M_v$	s.d.	$(b-v)_o$	s.d.	Ref.
WN6	-4.8	0.4	-0.28	0.02	1,2
WN7	-6.5	0.6	-0.27	0.05	1,2
WC4	-3.0		-0.30		2*,3

Table 5: Intrinsic parameters from the literature for relevant WR subtypes

References are 1: vdH (1995), 2: vdH *et al.* (1988), 3: Smith *et al.* (1990), \*: value extrapolated

### 6.1.1 WR 38

WR 38 was classified as a WC4 type Wolf-Rayet star by Lundström and Stenholm (1984a), Torres-Dodgen and Massey (1988) and Smith *et al.* (1990). As the first WC4 type star found in a Galactic open cluster, it offers a unique opportunity for deriving the intrinsic parameters of a WC4 star. Findings from other photometric studies are listed in Table 6. Other than for the values derived in this thesis (reference 4), the estimates of absolute magnitude and intrinsic colour are those adopted by the listed authors to obtain colour excess and distance information, with one exception. The exception is the distance-line flux calibration method used by Smith *et al.* (1990) to derive the value listed in Table 6 (reference 3b).

The absolute magnitude of WR 38,  $M_v = -5.1$ , is two magnitudes more luminous than has generally been adopted previously for WC4 type stars. Our estimate is uncertain, especially given the uncertainty in the reddening and distance of cluster stars. Yet the cluster colour-magnitude diagram produced by assuming a constant colour excess and a distance modulus  $v_o - M_v = 15.5$  is a good match to the colour-magnitude diagrams for other young open clusters. A decrease in the cluster's colour excess, or the distance modulus, or both would increase the estimated absolute magnitude for WR 38, but would also affect the absolute magnitudes and intrinsic colours of other cluster members. They would then be both redder and intrinsically less luminous, which would be inconsistent with a cluster containing a WR member.

It may be that WR 38 is not as highly reddened as other cluster members, but a difference of a tenth of a magnitude in colour excess will only decrease

$v_o$  by 0.2 magnitude. It appears therefore that the high luminosity we find for this star is not the result solely of an uncertainty in the star’s colour excess. There is some uncertainty in the cluster reddening, so the intrinsic colour of  $(b-v)_o = -0.42$  derived for WR 38 is only an estimate and is not intended to raise questions about published calibrations of intrinsic colour for WC4 stars.

$v$	$b-v$	$E_{b-v}$	$v_o$	$(b-v)_o$	$v_o - M_v$	$M_v$	Ref
13.39	0.93	1.23	8.47	-0.30*	11.5	-3.0*	1
15.6	0.88	1.18	10.8	-0.30*	13.8	-3.0*	2
15.4	0.93	1.23	10.4	-0.30*	13.4	-3.0*	3a
					14.4		3b
15.5	0.90	1.32	10.4	-0.42	15.5	-5.1	4

Table 6: Photometric and derived intrinsic properties of WR 38

References are 1: van der Hucht *et al.* (1988), 2: Torres-Dodgen and Massey (1988), 3: Smith *et al.* (1990) a: synthetic filter photometry, b: distance from line flux calibration, 4: This thesis, assuming mean of  $v$  and  $b - v$  from Refs. 2 and 3a, \*: intrinsic parameters assumed in colour excess and distance calculations.

### 6.1.2 WR 38a

WR 38a was discovered to be a Wolf-Rayet star and classified as “somewhere between WN6 and WN7, but closer to the former” by Shara *et al.* (1991). Listed in Table 7 are the  $ubv$  photometric data derived through synthetic filter photometry by Shara *et al.* (1991), and the derived intrinsic parameters, under the assumption of membership in the distant Carina cluster. Values listed for the colour excess and distance modulus are from this thesis.

The absolute magnitude,  $M_v = -4.4$  of WR 38a is within one standard

deviation of the average value for WN6 type stars as listed in Table 5. Its absolute magnitude is also very close to that of a very well-studied WN6 type star: WR 67. A recent analysis by Turner (1996) finds WR 67 to have an absolute magnitude  $M_v = -4.48 \pm 0.10$ , which is in excellent agreement with the WN6 type star studied here.

The derived  $(b-v)_o$  colour index for WR 38a is much bluer than the adopted values for WN6 stars (Table 5). The discrepancy is also statistically significant, given the small standard deviation associated with the value tabulated by van der Hucht *et al.* (1988). It may be that WR 38a is not as highly reddened as other members of the distant cluster. If its intrinsic colour is actually  $(b-v)_o = -0.28$ , then it must have a colour excess of  $E_{B-V} = 1.34$ , several tenths of a magnitude smaller than adopted for other cluster members. Such an effect could be produced by differential reddening, especially given the distance to the cluster and the fact that WR 38a lies at one edge of the region studied. Because of the uncertainties associated with the photometry for other cluster members, it is difficult to make a more confident statement concerning the intrinsic colour of WR 38a. The possibility also exists that it is not a cluster member, but the agreement between its derived absolute magnitude as a cluster member and those found for other WN6 stars in clusters is too close to be ignored.

$v$	$b-v$	$E_{b-v}$	$v_o$	$(b-v)_o$	$v_o - M_v$	$M_v$
16.21 <sup>1</sup>	0.83 <sup>1</sup>	1.32 <sup>2</sup>	11.05	-0.49	15.5 <sup>2</sup>	-4.4

Table 7: Photometric and derived intrinsic properties of WR 38a

References are 1: Shara *et al.* (1991), 2: This thesis

### 6.1.3 WR 87 and WR 89

WR 87 and WR 89 were classified as WN7 type stars by Lundström and Stenholm (1984a), Torres-Dodgen and Massey (1988), and Vacca and Torres-Dodgen (1990). Included in Tables 8 and 9 are  $ubv$  photometric data reported by van der Hucht *et al.* (1988), as well as derived intrinsic parameters and absolute magnitudes for the stars, assuming cluster membership. Colour excesses and distance modulus are as found in this thesis.

The absolute magnitude derived here for WR 87 is within one standard deviation of the average for WN7 stars as listed in Table 5, while that for WR 89 is not. It would be useful to compute a new average absolute magnitude for WN7 type stars that incorporates our new data, but again that is difficult without a list of the stars and their absolute magnitudes used by van der Hucht (1995) to compile their estimate.

WR 87 and WR 89 are intrinsically slightly bluer than the average intrinsic colour for WN7 type stars listed in Table 5. The intrinsic colour of WR 87 does fall within one standard deviation of the average for WN7 stars, while that of WR 89 does not. By re-averaging the data for single WN7 stars as reported by van der Hucht *et al.* (1988), using the new values of  $(b-v)_o$  derived here, we calculate a mean intrinsic colour of  $\langle (b-v)_o \rangle = -0.28 \pm 0.03$  (s.d.) for WN7 stars.

$v$	$b-v$	$E_{b-v}$	$v_o$	$(b-v)_o$	$v_o - M_v$	$M_v$
12.59 <sup>1</sup>	1.34 <sup>1</sup>	1.64 <sup>2</sup>	6.50	-0.30	13.19 <sup>2</sup>	-6.69

Table 8: Photometric and derived intrinsic properties of WR 87

References are 1: van der Hucht *et al.* (1988), 2: This thesis

$v$	$b-v$	$E_{b-v}$	$v_o$	$(b-v)_o$	$v_o - M_v$	$M_v$	Ref
11.53 <sup>1</sup>	1.22 <sup>1</sup>	1.55 <sup>2</sup>	5.76	-0.33	12.8 <sup>2</sup>	-7.43	2

Table 9: Photometric and derived intrinsic properties of WR 89

References are 1: van der Hucht *et al.* (1988), 2: This thesis

## 6.2 Conclusions

The WR stars WR 87 and 89 are almost certainly members of the young open cluster HM 1 at a distance  $V_o - M_V = 13.19 \pm 0.16$ . The intrinsic values of  $M_v$  and  $(b-v)_o$  for both WR stars have been determined and are included in Tables 8 and 9. The stars are intrinsically as luminous as has been found on average for WN7 stars in Galactic open clusters and associations. They are also slightly bluer than found on average previously for WN7 stars, and it is on the basis of our new estimates that we calculate a new average of  $\langle (b-v)_o \rangle = -0.28 \pm 0.03$  for the WN7 spectral type.

Centred at  $l = 290^\circ 57$ ,  $b = -0^\circ 92$  is a young open cluster, IAU designation OCL 1104-610. It is at a distance modulus of  $V_o - M_V = 15.3 \pm 0.2$  and is estimated to be several Myr old. Its potential members include two WR stars, WR 38 and WR 38a, and several O and B stars. The likely membership of WR 38 in the cluster has led to the first independent measure for the absolute magnitude of a WC4 star, which we estimate to be  $M_v = -5.1$ . That is two magnitudes more luminous than has been assumed previously for Galactic WC4 stars. The derived absolute magnitude for WR 38a is  $M_v = -4.4$  as derived with respect to a cluster main sequence fit. The value agrees with the average absolute magnitude found for other WN6 stars in Galactic open

clusters and associations.

The derived extreme luminosity of WR 38 is difficult to resolve with the apparent trend of decreasing luminosity for late to early WC spectral type stars. Yet, evolutionary calculations for massive stars do predict high luminosity WC4 type stars, given a low metallicity and/or high mass-loss rates in the input physics. Calculations by Meynet *et al.* (1994) do predict WC4 type stars with luminosities up to  $10^6 L_{\odot}$ , which is the approximate luminosity of WR 38, assuming a bolometric correction of  $B.C. = -4.5$  as found by Smith *et al.* (1994) for WC stars.

The WC4 type stars in the Large Magellanic Cloud are examples of higher luminosity WC4 types stars produced in a low metallicity environment. The average absolute magnitude of a LMC WC4 type star is  $M_v = -4.5$ , which fits in with theoretical calculations for stars produced in an environment with a metallicity that is less than solar, but does not fit in with the apparent trend for WC stars in open clusters and associations in our Galaxy. Under the assumption of membership in an open cluster at Galactic longitude  $l = 290^{\circ}57$  and at a distance of 15.3 kpc, WR 38 is well outside the solar circle. Assuming there is a Galactic metallicity gradient with metallicity decreasing from Galactic centre to edge, the environment that produced the distant cluster would be most likely of lower metallicity than the solar environment. Therefore a high luminosity WC4 type member is not such an anomaly.

The reddening of cluster members is uncertain given their faintness and the photometric limits of this study, and precise data regarding the intrinsic colours of the two WR stars are difficult to obtain. A deeper survey of the region surrounding WR 38 and WR 38a is necessary to acquire an accurate

picture of the reddening of cluster members, as well as to confirm the distance to the cluster. That would provide more precise values for the intrinsic properties of the two WR stars.

# Chapter 1

## HM 1 data

Star	HM #	$V$	$B-V$	$U-B$	$E_{B-V}$	$(B-V)_o$	$V_o$	Comment
1	1	11.04	1.52	0.39	1.88	-0.31	5.92	WR 89, m
2	4	11.39	0.41	(0.27)				n
3	2	11.43	1.55	0.35	1.88	-0.33	6.17	O4 If+, m
4	5	11.44	0.55	(0.21)				n
5	6	11.68	1.55	0.32	1.88	-0.33	6.42	O5 If+, m
6	7	11.98	0.37	(-0.02)				n
7	3	12.01	1.69	0.57	1.98	-0.34	6.33	WR 87, m
8	8	12.51	1.58	0.35	1.89	-0.31	7.22	O8 Ib(f), m
9	12	12.57	1.54	0.37	1.84	-0.30	7.35	m
10	14	12.59	0.61	(0.49)				n
11		12.70	0.42	(0.30)				n
12	13	12.78	1.51	0.35	1.82	-0.31	7.68	O8 I:, m
13		12.86	1.62	0.19	2.01	-0.39	7.18	m
14	17	12.89	0.64	(0.19)				n
15	9	13.07	1.61	0.38	1.93	-0.32	7.61	m
16	16	13.18	1.79	0.53	2.11	-0.32	7.21	m
17	15	13.21	0.68	(0.21)				n
18		13.31	0.47	(0.06)				n
19	11	13.32	0.65	(0.24)				n
20		13.34	0.38	(0.30)				n
21	18	13.40	1.47	0.33	1.77	-0.30	8.39	m
22	20	13.44	1.34	(0.27)				n
23		13.58	0.81	(0.35)				n
24		13.66	1.11	(0.70)				n
25		13.72	0.87	(0.56)				n

Star	HM #	$V$	$B-V$	$U-B$	$E_{B-V}$	$(B-V)_o$	$V_o$	Comment
26		13.88	0.77	(0.23)				n
27		13.90	0.61	(0.48)				n
28	10	13.94	1.53	0.29	1.86	-0.33	8.68	m
29		14.08	0.71	(0.18)				n
31	19	14.13	1.56	0.39	1.86	-0.30	8.86	m
32		14.22	1.03	(0.75)				n
33		14.28	0.73	(0.31)				n
34		14.31	2.72	(0.45)				n
35		14.38	0.77	(0.31)				n
36		14.39	1.76	(1.24)				n
37		14.40	1.85	(1.11)				n
38		14.44	1.64	0.48	1.94	-0.30	8.94	m
39		14.46	0.87	(0.30)				n
40		14.50	1.26	(0.78)				n
41		14.56	1.77	(1.22)				n
42		14.58	1.30	(0.85)				n
43		14.64	1.71	0.56	2.00	-0.29	8.99	m
44?		14.65	1.04	(0.74)				n
45		14.70	1.50	0.46	1.76	-0.26	9.71	m
46		14.73	1.67	0.25	2.05	-0.38	8.93	m
47		14.76	1.84	0.65	2.13	-0.29	8.73	m
48		14.79	0.68	(0.25)				n
49		14.82	0.75	(0.56)				n
50		14.88	1.03	(0.52)				n
51		14.89	0.79	(0.58)				n
52		14.94	0.81	(0.51)				n
53		14.99	1.70	0.52	2.00	-0.30	9.34	m
54		15.00	0.91	(0.48)				n
55		15.00	1.73	0.50	2.04	-0.31	9.22	m

Star	HM #	$V$	$B-V$	$U-B$	$E_{B-V}$	$(B-V)_o$	$V_o$	Comment
56	23	15.02	1.47	0.35	1.76	-0.29	10.03	m
57		15.02	1.20	(0.53)				n
58		15.10	0.96	(0.66)				n
59		15.11	1.14	(1.17)				n
60		15.12	0.84	(0.40)				n
61		15.14	1.47	(0.95)				n
62		15.15	2.42	(0.97)				n
63		15.17	1.63	0.40	1.95	-0.32	9.65	m
64		15.22	1.68	0.34	2.03	-0.35	9.47	m
65		15.25	1.00	(0.70)				n
66		15.25	1.57	0.52	1.83	-0.26	10.06	m
67		15.28	1.53	0.46	1.80	-0.27	10.18	m
68		15.29	0.83	(0.37)				n
69		15.29	0.81	(0.31)				n
70		15.29	1.30	(0.92)				n
71		15.34	1.84	0.62	2.14	-0.30	9.28	m
72		15.36	0.93	(0.46)				n
73		15.38	0.93	(0.69)				n
74		15.38	0.80	(0.34)				n
75		15.39	1.19	(0.52)				n
76		15.44	1.47	(0.98)				n
77		15.44	1.32	(0.89)				n
78		15.45	0.85	(0.33)				n
79		15.45	0.92	(0.21)				n
80		15.50	1.59	0.37	1.91	-0.32	10.10	m
81		15.50	2.33	(1.08)				n
82		15.51	1.13	(0.76)				n
83		15.52	1.65	0.64	1.89	-0.24	10.16	m
84		15.53	0.95	(0.68)				n
85		15.56	1.60	(0.34)				n

Star	HM #	$V$	$B-V$	$U-B$	$E_{B-V}$	$(B-V)_o$	$V_o$	Comment
86		15.56	1.27	(0.84)				n
87		15.56	0.95	(0.60)				n
88		15.56	1.20	(0.52)				n
89		15.62	1.12	(0.78)				n
90		15.65	1.53	0.60	1.75	-0.22	10.68	m
91		15.66	0.95	(0.61)				n
92		15.67	1.07	(0.58)				n
93		15.71	1.11	(0.54)				n
94		15.72	1.70	0.64	1.96	-0.26	10.18	m
95		15.73	1.50	(0.82)				n
96		15.78	1.80	0.58	2.10	-0.30	9.82	m
97		15.78	1.58	0.60	1.82	-0.24	10.64	m
98		15.79	1.00	(0.97)				n
99		15.79	2.15	(1.02)				n
100		15.80	1.58	0.48	1.86	-0.28	10.54	m
101		15.82	1.27	(0.79)				n
102		15.82	1.57	0.54	1.82	-0.26	10.65	m
103		15.87	1.61	0.47	1.90	-0.29	10.49	m
104		15.88	0.98	(0.39)				n
105		15.89	0.93	(0.68)				n
106		15.89	1.19	(1.23)				n
107		15.90	1.15	(0.78)				n
108		15.92	1.20	(0.67)				n
109		15.96	0.96	(0.73)				n
110		16.01	1.48	(1.01)				n
111		16.01	1.36	(0.88)				n
112		16.06	0.88	(0.42)				n
113		16.06	1.21	(0.82)				n
114		16.07	1.53	(0.95)				n
115		16.08	1.36	(0.69)				n

Star	HM #	$V$	$B-V$	$U-B$	$E_{B-V}$	$(B-V)_o$	$V_o$	Comment
116		16.09	1.52	()				n
117		16.09	1.04	(0.73)				n
118		16.10	1.42	()				n
119		16.13	1.35	(0.83)				n
120		16.15	1.14	(0.74)				n
121		16.17	0.95	(0.44)				n
122		16.18	1.17	(0.78)				n
123		16.18	1.17	(0.86)				n
124		16.20	1.19	(0.75)				n
125		16.24	0.93	(0.64)				n
126		16.25	1.50	()				n
127		16.26	1.05	(0.52)				n
128		16.27	1.46	()				n
129		16.29	1.03	(0.49)				n
130		16.29	1.18	(0.53)				n
131		16.30	1.26	(0.83)				n
132		16.30	1.11	(0.73)				n
133		16.31	1.31	()				n
134		16.31	1.25	(0.72)				n
135		16.32	1.57	0.59	1.81	-0.24	11.20	m
136		16.35	0.89	(0.49)				n
137		16.38	2.15	()				n
138		16.41	1.39	()				n
139		16.42	0.89	(0.40)				n
140		16.43	1.34	()				n
141		16.44	1.64	(-0.21)				n
142		16.44	1.08	(0.69)				n
143		16.45	1.14	(0.64)				n
144		16.47	1.10	(0.60)				n
145		16.48	1.77	0.65	2.04	-0.27	10.70	m

Table 10: Photometric data for stars in the region of HM 1

# Chapter 2

## Photometric data for Carina region stars

Star	$V$	$B-V$	$U-B$	$E_{B-V}$	$(B-V)_o$	$V_o$	Comment
A1	14.66	1.28	0.65	1.60	-0.32	10.05	WR 38, WC4
A2	15.12	1.15	0.06	1.60	-0.45	10.51	WR 38a, WN6
A3	15.51	1.28	0.10	1.60	-0.32	10.90	
A4	15.90	1.27	-0.04	1.60	-0.33	11.29	
A5	16.21	1.23	-0.15	1.60	-0.37	11.60	
A6	16.34	1.29	0.23	1.60	-0.31	11.87	
A7	16.51	1.30	0.04	1.60	-0.30	11.90	
A8	16.56	1.33	0.08	1.60	-0.27	11.95	

Table 11: Photometric data for stars in the distant cluster in the Carina field

Star	$V$	$B-V$	$U-B$	$E_{B-V}$	$(B-V)_o$	$V_o$	Comment
1	9.23	1.05	0.84	0.26	0.79	8.47	m
2	10.94	0.48	(0.07)				n
3	11.18	1.19	(1.18)				n
4	11.47	0.17	-0.12	0.27	-0.10	10.68	m
5	11.63	0.12	-0.37	0.25	-0.16	10.73	m
6	11.99	0.16	-0.26	0.30	-0.14	10.75	m
7	12.10	1.13	(0.97)				n
8	12.16	1.93	(2.42)				n
9	12.19	0.28	0.25	0.30	0.02	11.31	m
10	12.73	1.62	(1.76)				n
11	12.74	0.13	-0.33	0.28	-0.15	11.92	m
12	12.90	1.29	(0.05)				n
13	13.00	0.37	(0.31)				n
14	13.06	0.46	(0.05)				n
15	13.14	0.33	0.24	0.33	0.00	12.17	m
16	13.55	0.53	0.26	0.27	0.25	12.76	m
17	13.55	1.28	(1.32)				n
18	13.57	0.42	(0.25)				n
19	13.57	0.26	0.18	0.27	-0.01	12.78	m
20	13.80	0.56	0.28	0.30	0.26	12.92	m
21	13.87	1.55	(0.71)				n
22	13.91	0.36	(0.28)				n
23	13.91	1.08	(0.84)				n
24	13.93	0.79	(0.33)				n
25	14.01	0.63	(0.12)				n

Star	$V$	$B-V$	$U-B$	$E_{B-V}$	$(B-V)_o$	$V_o$	Comment
26	14.06	0.65	(0.12)				n
27	14.11	0.29	0.22	0.29	0.00	13.26	m
28	14.19	1.85	(1.52)				n
29	14.23	1.57	(1.42)				n
30	14.36	1.26	(0.99)				n
31	14.40	0.42	0.31	0.28	0.14	13.58	m
32	14.42	0.68	0.19	0.27	0.41	13.63	m
33	14.45	0.84	(0.41)				n
34	14.46	0.59	0.28	0.31	0.28	13.55	m
35	14.52	0.41	0.33	0.30	0.11	13.64	m
36	14.56	0.81	(0.33)				n
37	14.56	0.91	(0.63)				n
38	14.59	0.30	0.26	0.27	0.03	13.80	m
39	14.59	0.26	0.05	0.32	-0.06	13.65	
41	14.67	0.47	0.28	0.27	0.20	13.88	m
42	14.70	0.76	0.18	0.27	0.49	13.91	m
43	14.77	0.42	(-0.52)				n
44	14.78	0.65	(0.12)				n
45	14.80	0.34	0.28	0.32	0.02	13.86	m
46	14.86	0.59	(0.18)				n
47	14.97	0.38	0.32	0.29	0.09	14.12	m
48	14.97	0.77	(0.43)				n
49	14.99	0.61	(0.06)				n
50	15.03	1.30	(1.10)			0	n
51	15.03	1.52	(1.30)				n
52	15.06	0.79	(0.40)				n
53	15.06	0.70	0.22	0.22	0.25	14.41	m
54	15.10	0.70	0.15	0.21	0.49	14.48	m
55	15.11	0.41	(0.31)				n

Star	$V$	$B-V$	$U-B$	$E_{B-V}$	$(B-V)_o$	$V_o$	Comment
56	15.12	0.66	(0.16)				n
58	15.15	1.53	(1.27)				n
59	15.16	0.46	0.31	0.28	0.18	14.34	m
60	15.17	0.84	(0.29)				n
61	15.22	0.52	0.23	0.26	0.26	14.46	m
62	15.23	0.98	(0.25)				n
63	15.24	1.45	(1.01)				n
64	15.29	0.69	(0.14)				n
65	15.32	0.48	(0.23)				n
66	15.33	0.51	0.27	0.27	0.24	14.54	m
67	15.34	0.43	0.31	0.28	0.15	14.52	m
68	15.43	0.83	(0.29)				n
69	15.45	0.55	0.19	0.22	0.33	14.80	m
70	15.46	0.78	(0.27)				n
71	15.48	1.31	(0.81)				n
72	15.48	1.07	(0.59)				n
73	15.49	0.72	(0.34)				n
74	15.50	0.73	0.22	0.31	0.42	14.59	m
75	15.51	0.73	0.17	0.26	0.47	14.75	m
77	15.51	0.81	(0.48)				n
78	15.54	0.50	0.26	0.26	0.24	14.78	m
79	15.55	0.56	0.23	0.26	0.30	14.79	m
80	15.56	0.79	0.21	0.31	0.48	14.65	m
81	15.58	0.52	(0.14)				n
82	15.60	0.46	0.30	0.30	0.16	14.72	m
83	15.61	0.90	(0.50)				n
84	15.63	0.62	0.19	0.25	0.37	14.90	m
85	15.66	0.71	(0.30)				n

Star	$V$	$B-V$	$U-B$	$E_{B-V}$	$(B-V)_o$	$V_o$	Comment
86	15.66	1.05	(0.90)				n
87	15.69	0.96	(0.51)				n
88	15.71	0.66	(0.08)				n
89	15.73	0.59	0.21	0.26	0.33	14.97	m
90	15.73	0.74	(0.32)				n
91	15.74	0.82	(0.27)				n
92	15.74	0.55	(0.30)				n
93	15.75	1.32	(0.82)				n
94	15.78	0.80	(0.23)				n
95	15.80	0.57	0.21	0.25	0.32	15.07	m
96	15.82	0.76	(0.12)				n
97	15.82	1.03	(0.46)				n
98	15.84	0.60	0.16	0.24	0.36	15.13	m
99	15.86	0.68	0.18	0.26	0.42	15.10	m
100	15.89	0.75	(0.12)				n
102	15.92	0.49	0.27	0.27	0.22	15.13	m
103	15.94	0.64	(0.15)				n
104	15.94	0.70	0.17	0.26	0.44	15.09	m
105	15.96	0.62	0.29	0.33	0.29	14.99	m
106	15.97	0.88	(0.42)				n
107	15.97	1.04	(0.98)				n
108	16.03	0.87	(0.37)				n
109	16.05	0.90	(0.43)				n
110	16.06	0.92	(0.33)				n
111	16.08	1.05	(0.74)				n
112	16.11	0.86	(0.19)				n
113	16.12	1.45	(0.11)				n
114	16.12	0.89	(0.41)				n
115	16.14	0.68	(0.30)				n

Star	$V$	$B-V$	$U-B$	$E_{B-V}$	$(B-V)_o$	$V_o$	Comment
116	16.15	0.84	(0.39)				n
117	16.19	0.69	0.28	0.34	0.35	15.20	m:
118	16.19	0.89	0.33	0.27	0.62	15.41	m:
120	16.22	0.68	(0.03)				n
121	16.23	0.57	0.27	0.30	0.27	15.36	m:
122	16.28	0.67	(0.32)				n
123	16.30	0.73	0.19	0.28	0.45	15.49	m:
124	16.31	0.82	(0.28)				n
125	16.32	0.80	(0.25)				n
126	16.32	0.70	(0.12)				n
128	16.35	0.80	(0.36)				n
129	16.38	0.67	(0.42)				n
130	16.40	0.68	0.18	0.26	0.42	15.65	m:
131	16.44	1.19	(0.12)				n
132	16.45	0.71	(0.10)				n
133	16.46	0.77	0.21	0.29	0.48	15.62	m:
134	16.49	0.82	(0.22)				n
135	16.49	0.82	(0.35)				n
136	16.49	0.74	(0.17)				n

Table 12: Photometric data for stars in the Carina region

# Chapter 3

## Possible Carina cluster

### C.1 Extinction

An extinction analysis for the Carina region was initially performed as outlined in Section 4.1. Twenty-one stars near the Carina region were chosen to examine the reddening. The data did not seem to fall along a tight linear trend as seen in Figure C.1. The formal result from fitting the data to a linear relation with no zero-point offset (the program `nulfit.f`) was to produce a reddening slope of  $E_{U-B}/E_{B-V} = 0.714 \pm 0.052$ . An attempt to separate the data into subgroups based upon spectral type or position did not help to explain the poor agreement. Analysis of a preliminary colour-colour diagram showed that for the cluster  $E_{B-V} \sim 0.3$ , so a reddening slope of 0.76 was adopted according to Equation 5.1 which has been shown to be valid for regions in Carina. The adopted value is within the formal uncertainty of the `nulfit.f` result, and does seem to fit the extrema of the data quite well.

### C.2 Star Counts

Star counts were performed as outlined in Section 4.2. An image of the region obtained from the Digitized Sky Survey was examined. Strips one arcminute in width were drawn on a hardcopy of the image vertically and then horizontally, so that stars could be counted in each strip to an arbitrary faintness limit on the image. The results are seen in Figures C.2 and C.3. Error bars have been constructed according to Poisson statistics. The measured centre is indicated on the main figure; it lies at  $l = 290^\circ.58$ ,  $b = -0^\circ.94$ . It appears

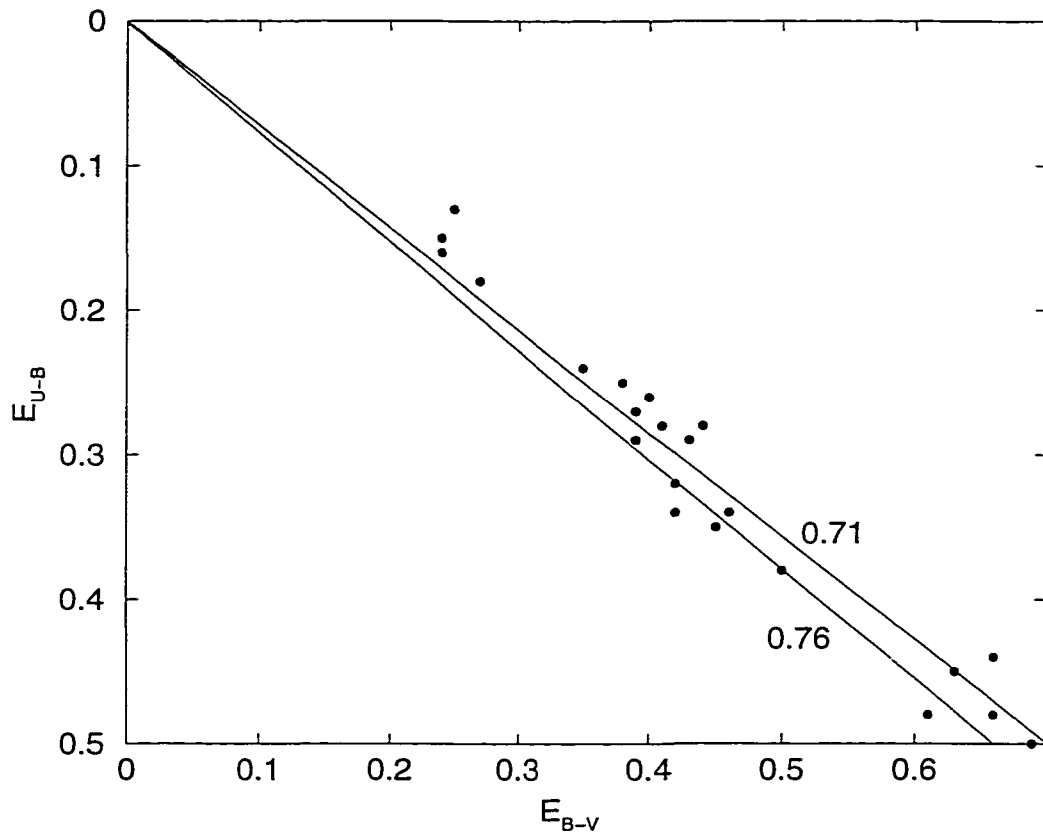


Figure C.1:  $E_{U-B}$  vs.  $E_{B-V}$  in the Carina region with lines of slope 0.71 and 0.76 drawn

that the number of stars increases towards the north and east. That may be a result of patchy extinction or perhaps a true increase in stellar density toward the galactic plane.

Ring counts were then performed with respect to the adopted centre. Rings were constructed in half arcminute radius intervals and stars were counted above the same faintness limit as the strip counts. The resulting stellar number density as a function of cluster radius is seen in Figure C.4. Error bars are constructed according to Poisson statistics. The cluster does not stand out distinctly above the background, but a central peak can be seen, as well as a background of 1.3 stars per square arcminute. A cluster radius of 2'.0 was adopted. The total number of stars counted within this radius is  $28 \pm 5$ , while one expects 18 background stars in the same region. One therefore expects roughly 30% of the observed stars to be cluster members. The stellar density may increase again beyond our adopted cluster radius, but that is most likely because of the increase in the number of stars toward the north.

Star counts were also made by constructing  $4' \times 4'$  square regions centred on the cluster and on random regions within 10' of the apparent cluster centre. Stars were counted above an arbitrary faintness limit and then compared. The region centred on the cluster was found to contain  $44 \pm 7$  stars, while the other regions were found to contain  $33 \pm 6$ ,  $36 \pm 6$ ,  $26 \pm 5$  and  $25 \pm 5$  stars (uncertainties are according to Poisson statistics), resulting in an average of  $30 \pm 5$  (s.d.) background stars. Here, a formal result shows that only  $32 \pm 20\%$  of the observed stars within the cluster boundary are cluster members. The uncertainty in the estimate is rather large, but it reinforces

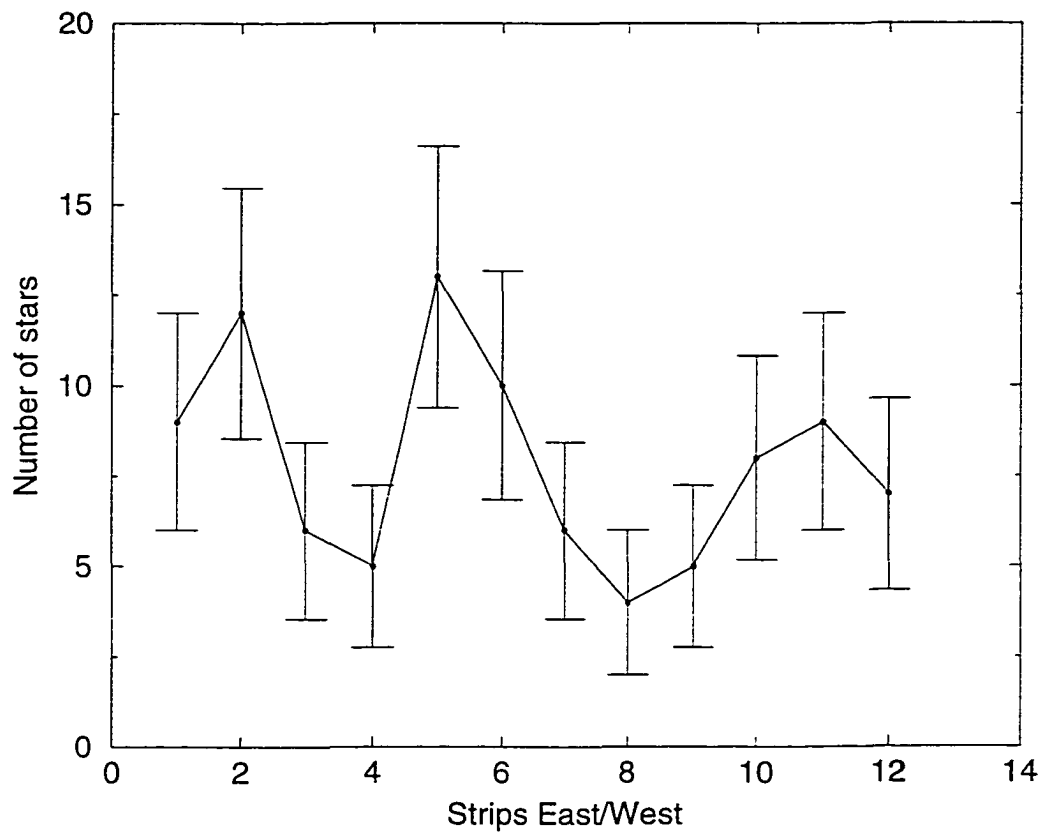


Figure C.2: Strip counts in east/west direction for the Carina region

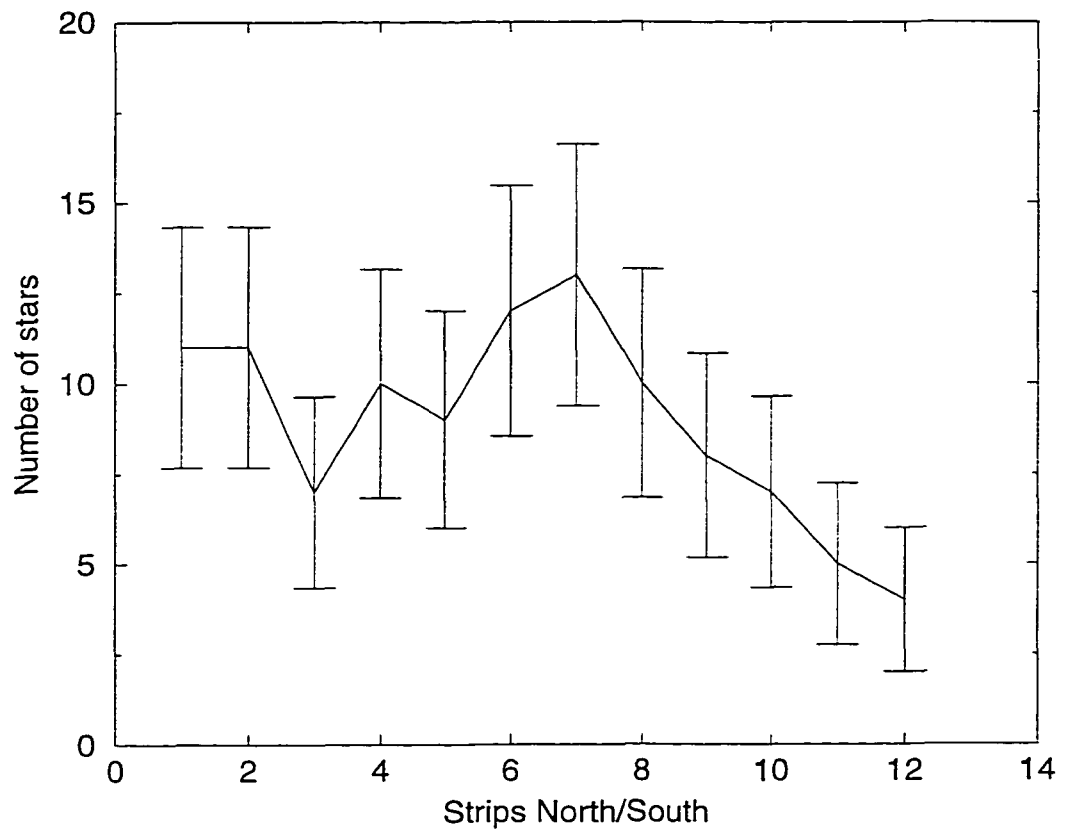


Figure C.3: Strip counts in north/south direction for the Carina region

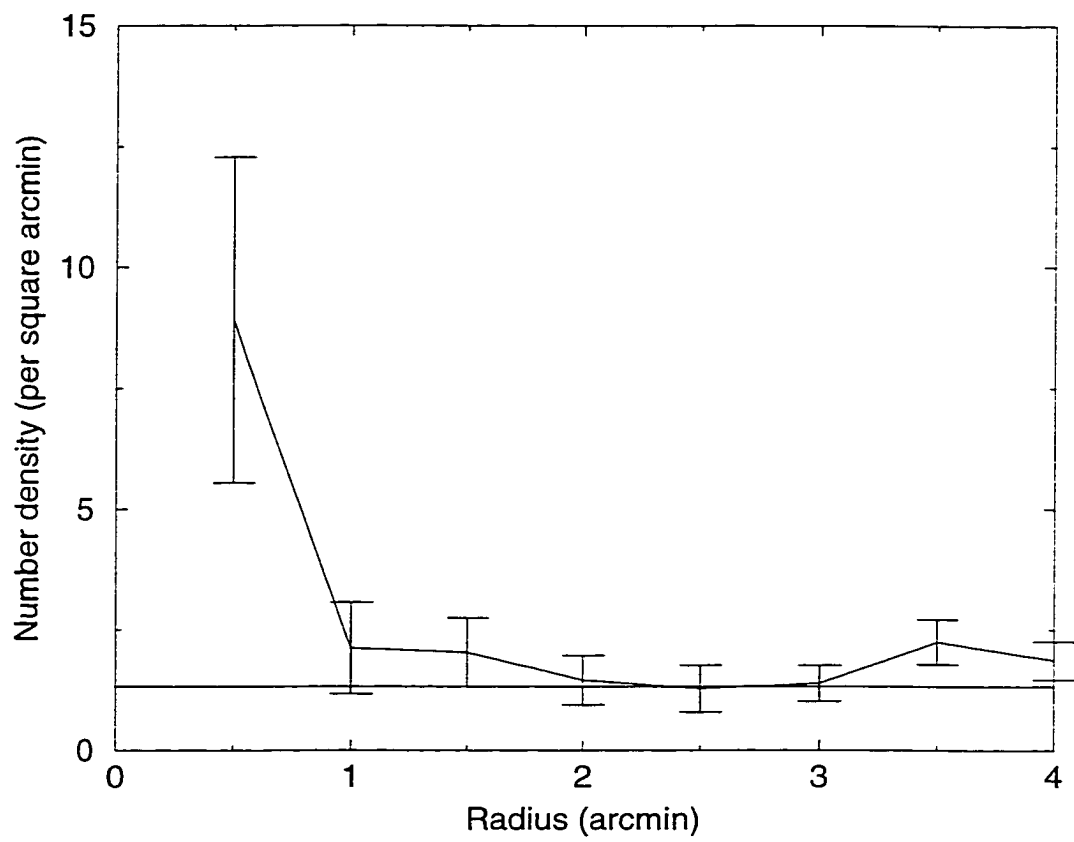


Figure C.4: Ring counts for the Carina region

the estimate of 30% based on ring counts. Having identified 136 individual stars in the Carina region with  $V < 16.5$ , one expects approximately 40 identified members.

### C.3 Colour-colour diagram

In order to determine what sort of correction should be applied to the  $U-B$  data, the colour-colour diagram for the cluster was examined to assign an approximate spectral type for each candidate star.

Initially the colour-colour diagram for the Carina region exemplified the problem with systematic errors in  $U-B$  and mimicked the CCD of Vázquez *et al.* (1994). The uncorrected version may be seen in Figure C.5. Reddened colour-colour relations with  $E_{B-V} = 0.25$  and  $E_{B-V} = 0.30$  have been plotted. The data clearly contain a reddened sequence ( $E_{B-V} \sim 0.3$ ), but the relation in the A0-A6 region is “flattened” somewhat. When a spectral type dependent correction was applied to the points, as outlined in Section 3.2.1, the usual distribution of data points outlining a reddened intrinsic relation was more apparent.

The correction was at first applied simply as a function of  $B-V$ , for a constant  $E_{B-V}$ . That was not completely appropriate, as several times stars were dereddened to different spectral types than those upon which the size of corrections were based. (*e.g.*, A star assumed to be A2 was given a correction appropriate to an A2 star. The star was then dereddened to an A1 colour.) To correct for that the procedure was repeated several times, using the new dereddened spectral types as a basis for the correction and thus allowing the solutions to converge.

Data points with  $B-V < 0.2$  were given a  $-0.03$  correction in  $U-B$  as they

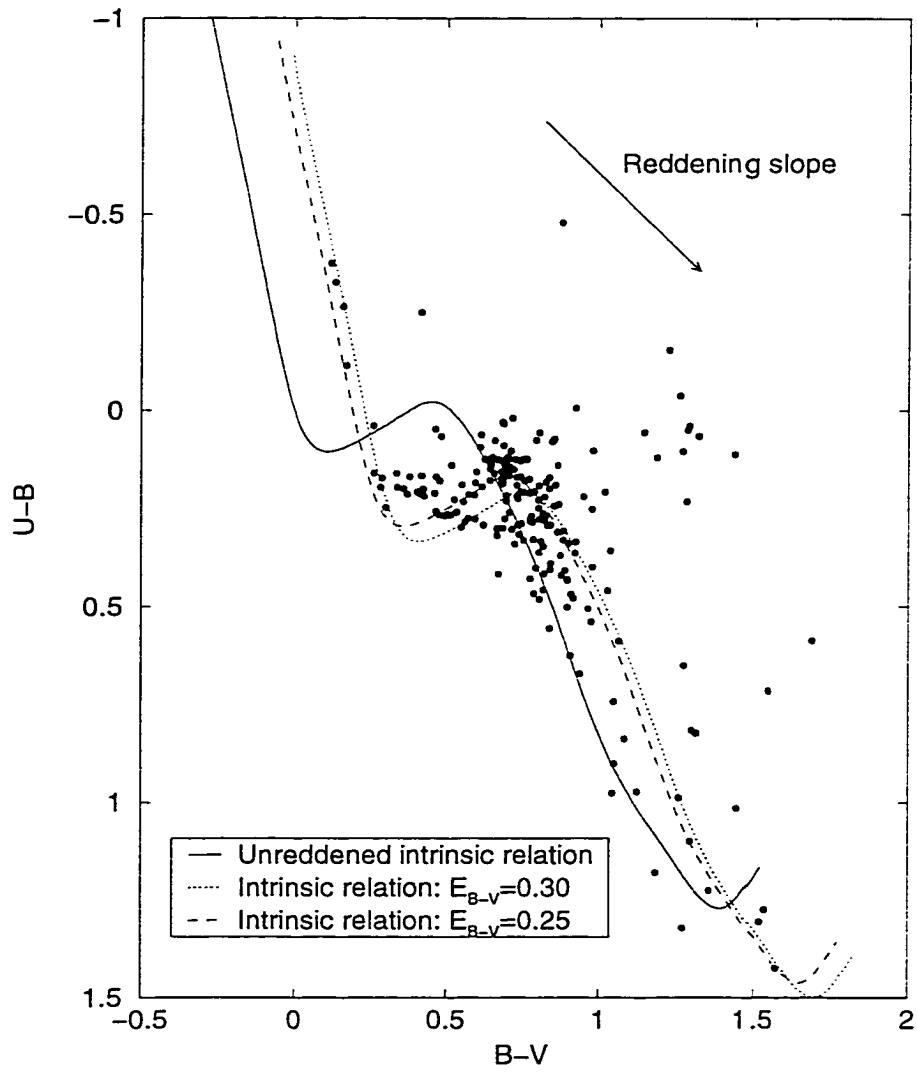


Figure C.5: Uncorrected colour-colour diagram for the Carina region

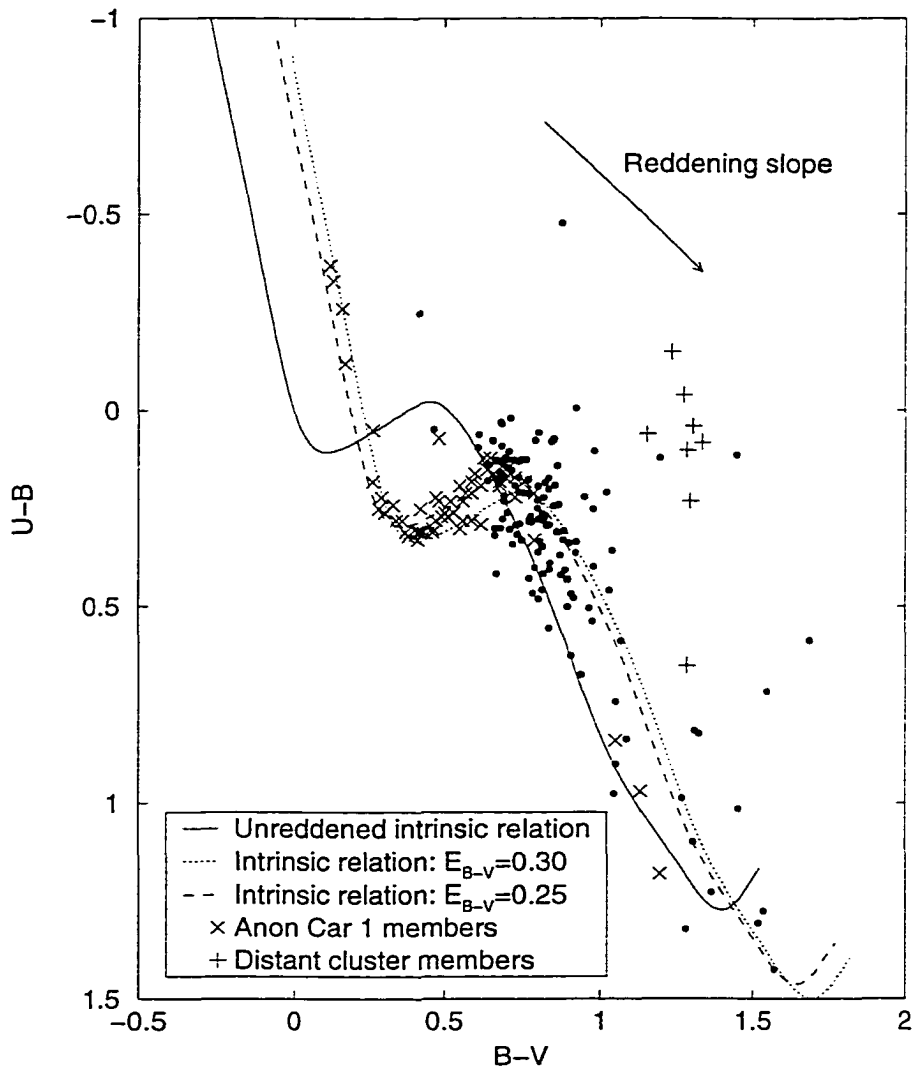


Figure C.6: Corrected colour-colour diagram for the Carina region

were dereddened to a spectral type earlier than B9. The corrected colour-colour diagram is shown in Figure C.6. Photometric data for all probable cluster members indicated by “m” under “Comments”, are listed in Appendix B, including corrected  $U-B$  values. Data for non-members are also included, indicated by “n” under “Comments”, but with  $U-B$  values in brackets indicating that they are approximate.

As is typical of colour-colour diagrams for sparse open clusters, there is a great deal of contamination from non-member stars. There is also a group of stars ( $0.7 < E_{B-V} < 0.9$  and  $0.1 < E_{U-B} < 0.2$ ) that could not be dereddened to the seemingly correct F-star region of the intrinsic relation using the reddening line of slope 0.76. While they could be highly reddened B stars, there are alternative explanations. They might also be metal-poor stars, in which case the intrinsic colour-colour relation used here would not have resulted in correct dereddening solutions. The stars are also near the limit of faintness for reliable photometry, and photometric errors, especially in  $U$ , may be responsible for their unusual location in the diagram. Finally, they may also be influenced by some systematic instrumental effect, similar to that affecting A-type stars, which is impossible to investigate without more data.

## C.4 Variable-Extinction Diagram

The variable-extinction diagram for candidate members in the Carina region, Figure C.7, shows a spread in  $V-M_V$  like that in HM 1, as well as the presence of a distinct group of data points corresponding to the possible highly-reddened cluster. Again the data seem to be consistent with a large value of  $R$ , but that may be explained by random scatter, especially for the

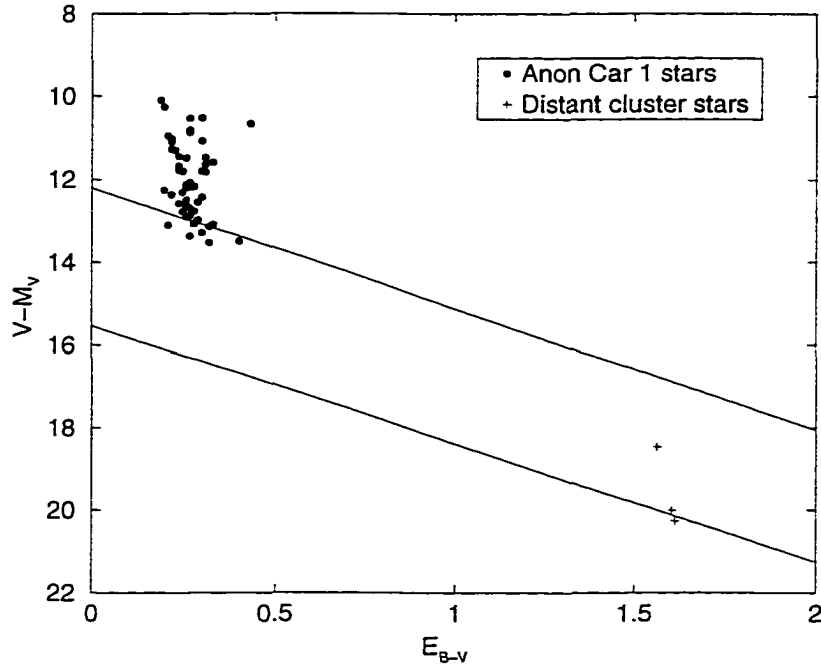


Figure C.7: Variable extinction diagram for the Carina region

hottest stars (Turner 1976a).

Since the value of  $R$  could not be accurately determined from the variable-extinction diagram, a value of  $R = 2.94$  was adopted according to Equation 4.7. Stars listed in Table 13 were used to calculate the mean distance modulus  $\langle V_o - M_V \rangle = 12.02 \pm 0.06(\text{s.e.})$ . The brightest candidate cluster members were excluded as they were possibly not main sequence objects. Several other candidate members were excluded since their values of  $V_o - M_V$  were probably affected by binarity and rapid rotation, as expected for a sample of open cluster stars.

Star	$V$	$B-V$	$U-B$	$E_{B-V}$	$(B-V)_o$	$V_o$	$V_o - M_V$
38	14.59	0.30	0.26	0.27	0.03	13.80	12.09
45	14.80	0.34	0.28	0.32	0.02	13.86	12.20
47	14.97	0.38	0.32	0.29	0.09	14.12	12.13
53	15.06	0.70	0.22	0.22	0.25	14.41	11.72
59	15.16	0.46	0.31	0.28	0.18	14.34	11.95
61	15.22	0.52	0.23	0.26	0.26	14.46	11.73
66	15.33	0.51	0.27	0.27	0.24	14.54	11.90
67	15.34	0.43	0.31	0.28	0.15	14.52	12.25
69	15.45	0.55	0.19	0.22	0.33	14.80	11.72
78	15.54	0.50	0.26	0.26	0.24	14.78	12.14
79	15.55	0.56	0.23	0.26	0.30	14.79	11.86
82	15.60	0.46	0.30	0.30	0.16	14.72	12.41
84	15.63	0.62	0.19	0.25	0.37	14.90	11.58
89	15.73	0.59	0.21	0.26	0.33	14.97	11.89
95	15.80	0.57	0.21	0.25	0.32	15.07	12.04
98	15.84	0.60	0.16	0.24	0.36	15.13	11.87
102	15.92	0.49	0.27	0.27	0.22	15.13	12.58
105	15.96	0.62	0.29	0.33	0.29	14.99	12.12
117	16.19	0.69	0.28	0.34	0.35	15.20	12.01
121	16.23	0.57	0.27	0.30	0.27	15.36	12.58
123	16.30	0.73	0.19	0.28	0.45	15.49	11.60
130	16.40	0.68	0.18	0.26	0.42	15.65	11.97

Table 13: Photometric data for stars in the Carina region used to estimate  $V_o - M_V$

A preliminary reddening map for candidate members of the Carina region shows possible variations in reddening across the cluster region, with a mean of  $\langle E_{B-V} \rangle = 0.27$ . Stars with colour excesses as low as 0.15 and as high as 0.50 were not immediately eliminated as members, but a range  $0.25 < E_{B-V} < 0.35$  seemed to describe the data best. Stars with two possible colour excesses from the dereddening process were compared with neighbouring stars and either one of the values was chosen if it was similar to the reddening of

nearby stars or the star was marked a non-member if no comparable values were obtained. The final reddening map is seen in Figure C.8.

All values of  $E_{B-V}$  and the corresponding values of  $(B-V)_o$  are included in Appendix B. In order to ensure that no information was lost, all stars with colour excesses in the range  $0.15 < E_{B-V} < 0.50$  were included to construct a preliminary colour-magnitude diagram, but those not falling within the tighter range given above were marked as non-members.

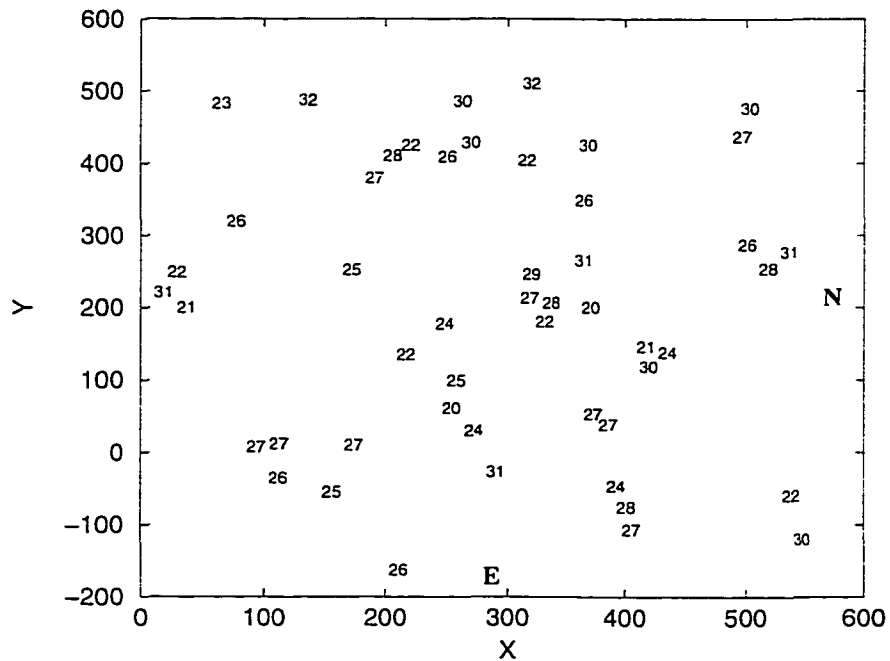


Figure C.8: Reddening Map of the Carina region based upon colour excesses in units of  $0^m.01$  in  $E_{B-V}$

## C.5 Colour-magnitude diagram

The colour-magnitude diagram for the Carina region, Figure C.9, roughly outlines a main sequence with evolved stars, but contamination from field stars makes a tight sequence difficult to isolate. The star counts indicate that only thirty per cent of all stars should be members of the cluster, so it is obvious that not all stars included in Figure C.9 can be members. The data were sorted by colour excess to determine which stars could be excluded. The sorting is seen in Figure C.10. Stars with the smallest and largest colour excesses are most obviously not members, confirming what is evident from examination of the reddening across the cluster region. Several stars with colour excesses in the range  $0.20 < E_{B-V} < 0.35$  do not fit the expected CMD plot very well, but have been included anyway. The total number of stars with appropriate reddenings is 41, which is consistent with the star counts. A ZAMS line for  $V_o - M_V = 12.02$  is a reasonable fit to the cluster data and confirms the value from the variable extinction analysis.

Based upon a comparison of the data with isochrones by Meynet *et al.* (1993), the cluster CMD is indicative of an intermediate age open cluster. With that in mind, we re-examined the possibly evolved cluster member; star number 1. Its intrinsic colour was not adopted on the basis of dereddening to the intrinsic two-colour relation but upon the colour excesses of surrounding stars. Spectroscopic data for the star could not be found in the literature, even though such data would have assisted in the assignment of an intrinsic colour and absolute magnitude.

The MSTO is difficult to establish with only one data point on the main sequence near what appears to be the turn-off. An isochrone for  $t = 77$  Myr

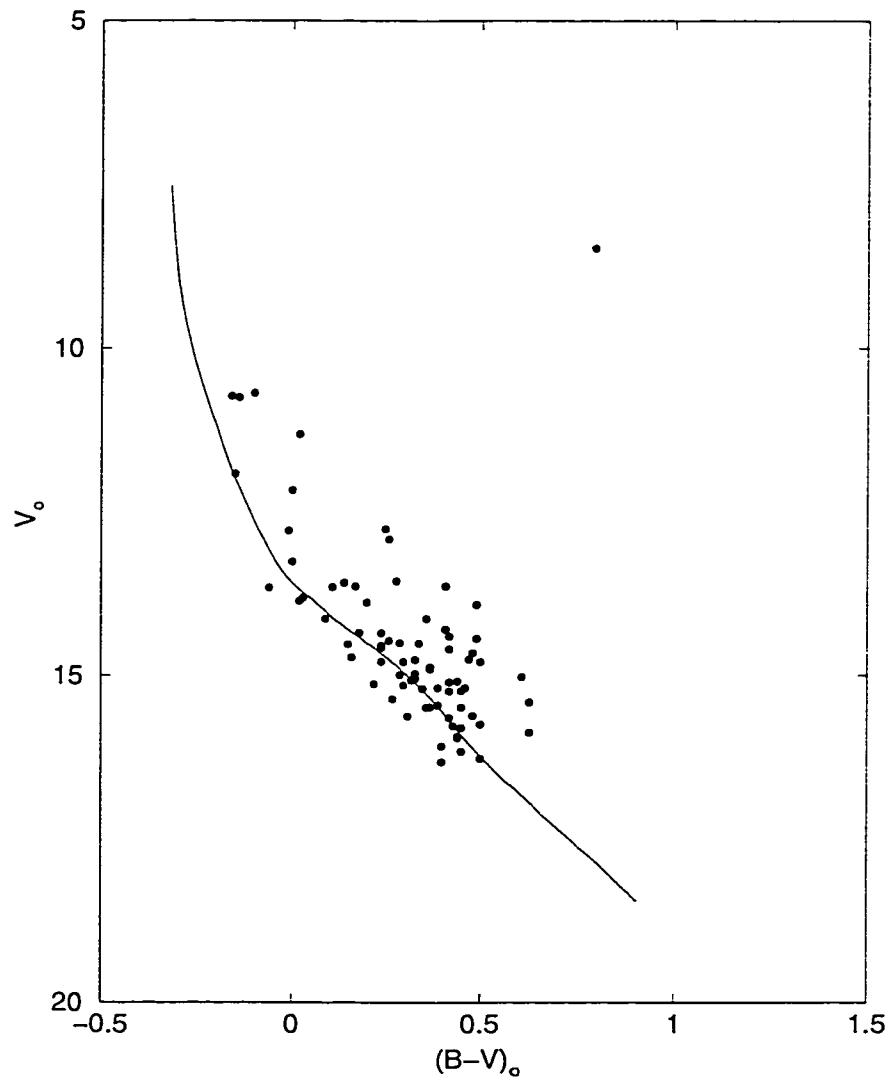


Figure C.9: Colour Magnitude Diagram for the Carina region.

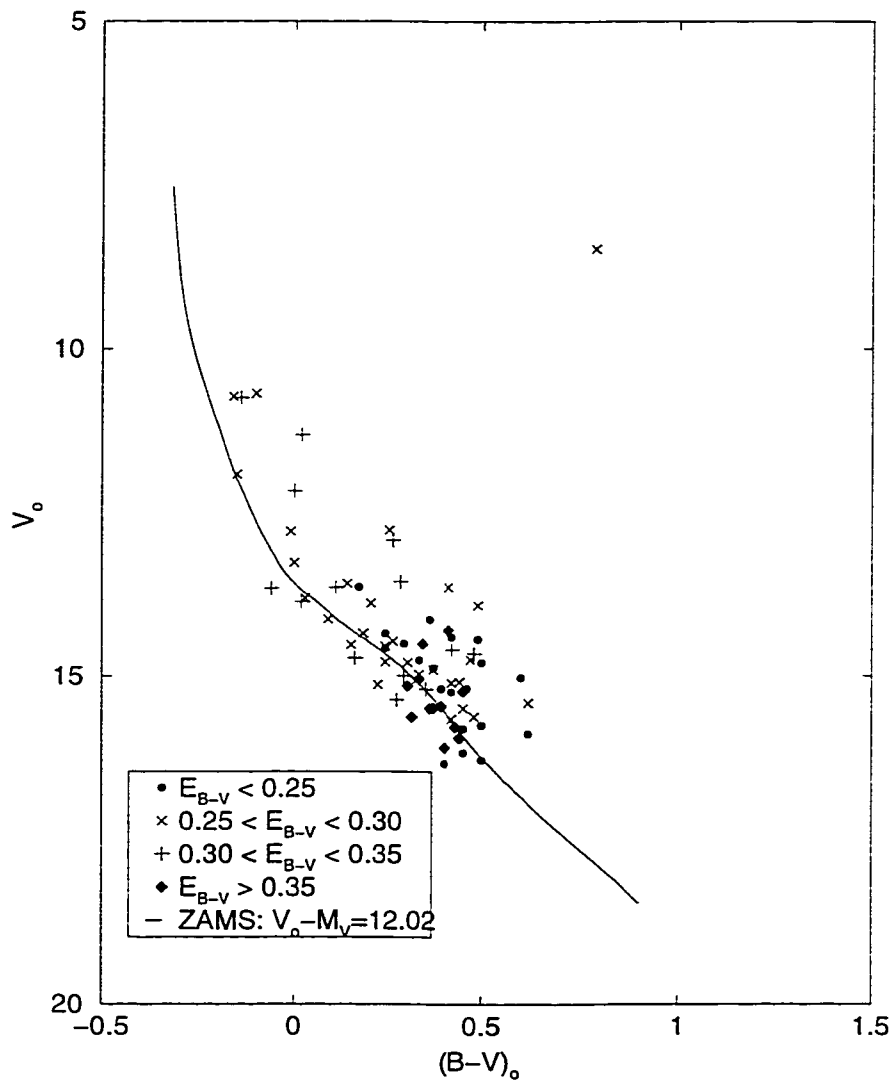


Figure C.10: CMD for the Carina region with stars categorized by colour excess

has been overlain on the plot, Figure C.11, as a best match to the upper end of the main sequence and to the slightly evolved stars just above the main sequence. The MSTO corresponding to  $t = 77$  Myr lies at  $(B-V)_o = -0.155$  (Turner, private communication), which is entirely consistent with the data. The 77 Myr isochrone also matches the point corresponding to star number 1 quite well. It appears that star number 1 may be a cluster member, possibly a yellow supergiant.

There is considerable scatter within the points that may or may not be attributable to contamination from non-members as well as binarity or photometric error. Given the sparseness of the cluster, contamination must be large and is the most likely source of the scatter. Uncorrected spectral type dependent effects may also play a role. Although such problems seem considerable, resolving them is not crucial because the nearest Carina region cluster is not the focus of this thesis.

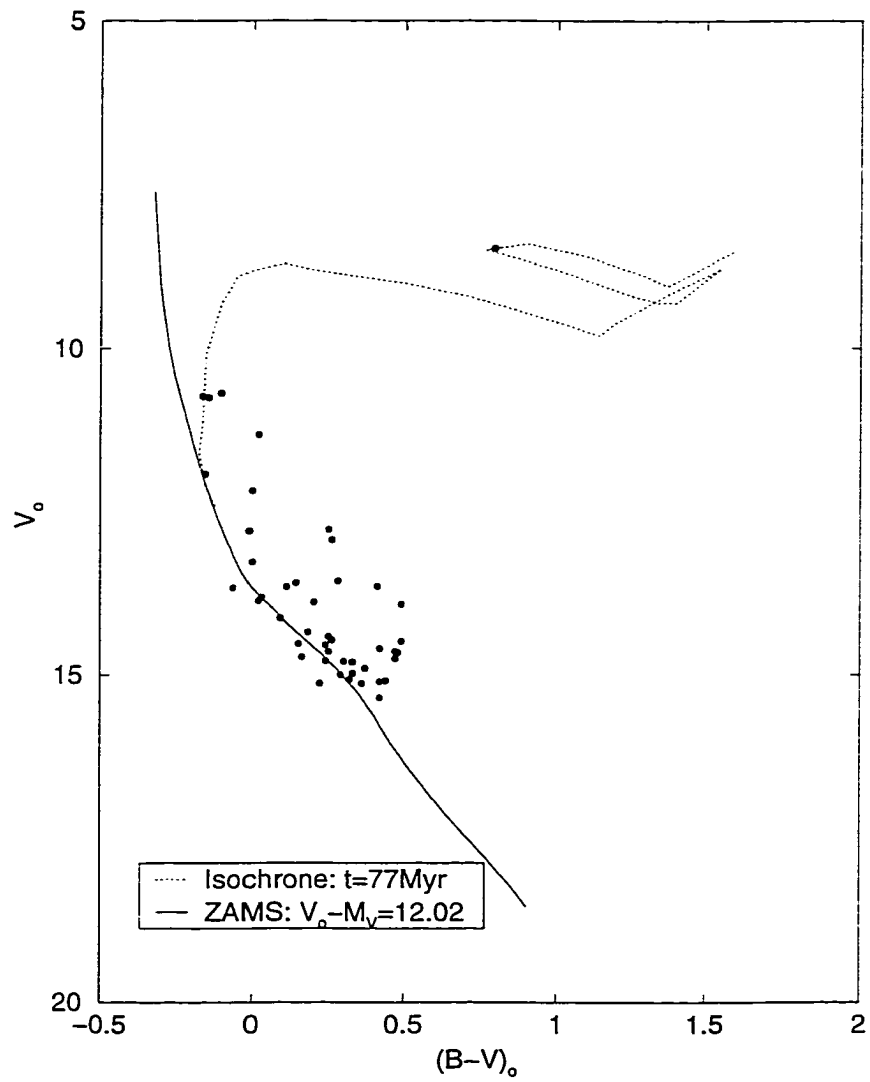


Figure C.11: CMD for Carina region cluster members with overlaid isochrone

## References

- Allen, C. W. (1973) *Astrophysical Quantities*, (Athlone Press: London)
- Bessell, M. S. (1990) *Publications of the Astronomical Society of Pacific*, **102**, No. 656, 1181.
- Bessell, M. S. (1993) in: Butler, C. J. and Elliott, I. (eds.) *Stellar Photometry - Current Techniques and Future Developments Proceedings of IAU Colloquium No. 136*, (Cambridge University Press: Cambridge), p. 22.
- Conti, P. S. (1996) in: Vreux, J. M. *et al.* (eds.) *Wolf-Rayet Stars in Framework of Stellar Evolution. Proceedings of the 33rd Liège International Astrophysical Colloquium*, (Liège: Université de Liège) p. 655.
- Conti, P. S. and Vacca, W. D. (1990) *Astronomical Journal*, **100**, 431.
- Drilling, J. S. (1991) *Astrophysical Journal Supplement Series*, **76**, 1033.
- Forbes, D. and Short, S. (1996) *Astronomical Journal*, .
- Garrison, R. F., Hiltner, W. A. and Schild, R. E. (1977) *Astrophysical Journal Supplement Series*, **35**, 111.
- Havlen, R. J. and Moffat, A. F. J. (1977) *Astronomy and Astrophysics*, **58**, 351.
- Johnson, H. L. (1953) in: Strand, K. A. (ed.) *Basic Astronomical Data*, (University of Chicago Press: Chicago) p. 204.

- Klare, G. and Neckel, Th. (1977) *Astronomy and Astrophysics Supplement Series*, **27**, 215.
- Klare, G. and Szeidl, B. (1966) *Veroeff. des Badischen Sternw. Heidelberg*, **18**, 9.
- Lundström, I. and Stenholm, B. (1984a) *Astronomy and Astrophysics Supplement Series*, **56**, 43.
- Lundström, I. and Stenholm, B. (1984b) *Astronomy and Astrophysics Supplement Series*, **58**, 163.
- Massey, P. (1984) *Astrophysical Journal*, **281**, 789.
- Massey, P. and Davis, L. E. (1992) *A User's Guide to Stellar CCD Photometry with IRAF*
- Meynet, G., Maeder, A., Schaller, G., Schaerer, D., and Charbonnel, C. (1994) *Astronomy and Astrophysics Supplement*, **103**, 97.
- Meynet, G., Mermilliod, J. C., and Maeder, A. (1993) *Astronomy and Astrophysics Supplement Series*, **98**, 477.
- Moffat, A. F. J. and Vogt, N. (1975) *Publications of the Astronomical Society of Pacific*, **20**, 155.
- Moffat, A. F. J. and Vogt, N. (1977) *Publications of the Astronomical Society of Pacific*, **89**, 323.
- Schild, R. E., Garrison, R. F. and Hiltner, W. A. (1983) *Astrophysical Journal Supplement Series*, **51**, 321.
- Shara, M. M., Moffat, A. F. J., Smith, L. F., and Potter, M. (1991) *Astronomical Journal*, **102**, 716.

- Shelton, I. (1996) Ph. D. thesis, University of Toronto.
- Smith, L. F. (1968) *Monthly Notices of Royal Astronomical Society*, **138**, 109.
- Smith, L. F., Meynet, G. and Mermilliod, J. C. (1994) *Astronomy and Astrophysics*, **287**, 835.
- Smith, L. F., Shara, M. M., and Moffat, A. F. J. (1990) *Astrophysical Journal*, **358**, 229.
- Smith, L. F., Shara, M. M., and Moffat, A. F. J. (1996) *Monthly Notices of the Royal Astronomical Society*, **281**, 163.
- Straižys, V. and Lazauskaitė, R. (1995) *Baltic Astronomy*, **4**, No. 1, 88.
- Torres-Dodgen, A. V. and Massey, P. (1988) *Astronomical Journal*, **96**, 1076.
- Turner, D. G. (1976a) *Astronomical Journal*, **81**, 97.
- Turner, D. G. (1976b) *Astronomical Journal*, **81**, 1125.
- Turner, D. G. (1980) *Astrophysical Journal*, **240**, No. 1, 137.
- Turner, D. G. (1981) in: de Loore, C. W. H. and Willis, A. J. (eds.) *Wolf-Rayet Stars: Observations, Physics, Evolution. Proceedings of the 99th Symposium of International Astronomical Union*, (Dordrecht: D. Reidel) p.57.
- Turner, D. G. (1996) *Astronomical Journal*, **111**, 828.
- Vacca, W. D. and Torres-Dodgen, A. V. (1990) *Astrophysical Journal Supplement Series*, **73**, 685.

- van den Bergh, S. and Sher, D. (1960) *Publications of the David Dunlap Observatory*, **2**, 203.
- van der Hucht, K. A., Conti, P. S., Lundström, I. and Stenholm, B. (1981) *Space Science Reviews*, **28**, 227.
- van der Hucht, K. A., Hidayat, B., Admiranto, A. G., Supelli, K. R., and Doom, C. (1988) *Astronomy and Astrophysics*, **199**, 217.
- van der Hucht, K. A. (1995) in: van der Hucht, K. A. and Williams, P. M. (eds.) *Wolf-Rayet Stars: Binaries, Colliding Winds, Evolution. Proceedings of the 163rd Symposium of International Astronomical Union*, (Dordrecht: Kluwer) p. 7.
- van der Hucht, K. A. (1996) in: Vreux, J. M. *et al.* (eds.) *Wolf-Rayet Stars in Framework of Stellar Evolution. Proceedings of the 33rd Liège International Astrophysical Colloquium*, (Liège: Université de Liège) p. 1.
- Vázquez, R. A., Baume, G., Feinstein, A. and Prado, P. (1994) *Astronomy and Astrophysics Supplement Series*, **106**, 339.
- Vázquez, R. A., Baume, G., Feinstein, A. and Prado, P. (1997) *Astronomy and Astrophysics Supplement Series*, **124**, 13.
- Vázquez, R. A., Will, J. M. G., Prado, P. and Feinstein, A. and (1995) *Astronomy and Astrophysics Supplement Series*, **111**, 85.
- Westerlund, B. E. (1966) *Astrophysical Journal*, **145**, 724.

## Vita

Name: Stephen Lawrence Shorlin

Place of Birth: Corner Brook, Newfoundland

Year of Birth: 1973

Education: Memorial University of Newfoundland  
St. John's, Newfoundland  
1995 B. Sc. (Hons.) in Physics

Saint Mary's University  
Halifax, Nova Scotia  
1998 M. Sc. in Astronomy

Related Experience: Guest Observer  
University of Toronto Southern Observatory  
June, 1996

### Publications:

- "Pismis 6 and the F0 Ia Supergiant HD 74180" with D. Forbes,  
1994, AJ, 108, 594.
- "NGC 6204 and Hogg 22: The Odd Couple" with D. Forbes, 1996, AJ,  
111, 1609.